Bedrock Infiltration Estimates from a Catchment Water Storage-Based Modeling Approach in the Rain Snow Transition Zone

Patrick R. Kormos, James P. McNamara, Mark S. Seyfried, Hans Peter Marshall, Danny Marks, Alejandro N. Flores

PII: S0022-1694(15)00203-6
DOI: http://dx.doi.org/10.1016/j.jhydrol.2015.03.032
Reference: HYDROL 20326

To appear in: *Journal of Hydrology*

Received Date: 1 October 2014
Revised Date: 12 March 2015
Accepted Date: 14 March 2015

Bedrock Infiltration Estimates from a Catchment Water Storage-Based Modeling Approach in the Rain Snow Transition Zone.

Patrick R. Kormos[1, 2, 3, 4] phone: 001-208-921-1930 email: patrick.kormos@ars.usda.gov
James P. McNamara[1]
Mark S. Seyfried[4]
Hans Peter Marshall[1]
Danny Marks[4]
Alejandro N. Flores[1]

1. Department of Geosciences, Boise State University, 1910 University Dr., Boise, ID 83725, USA
2. Rocky Mountain Research Station, U.S. Forest Service, 322 E. Front St., Suite 401, Boise, ID, 83702, USA
3. Oak Ridge Institute for Science and Education, P.O. Box 117, Oak Ridge, TN, 37831, USA
4. Northwest Watershed Research Center, U.S. Agricultural Research Service , 800 E. Park Blvd., Suite 105, Boise, ID 83712, USA

FIRST PAGE FOOTER: *Abbreviations: BI - bedrock infiltration, ROS – rain on snow, DR – drainage to the soil bedrock interface, SWI – surface water inputs, NE – northeast-facing, SW – southwest-facing*

Abstract

Estimates of bedrock infiltration from mountain catchments in the western U.S. are essential to water resource managers because they provide an estimate of mountain block recharge to regional aquifers. On smaller scales, bedrock infiltration is an important term in water mass balance studies, which attempt to estimate hydrologic states and fluxes in watersheds with fractured or transmissive bedrock. We estimate the a daily time series of bedrock infiltration in a small catchment in the rain snow transition zone in southwest Idaho, using the difference between measured stream discharge and modeled soil drainage. The accuracy of spatial patterns in soil water storage are optimized, rather than the more common approach of minimizing error in integrated quantities such as streamflow. Bedrock infiltration is estimated to be 289 mm ± 50 mm for the 2011 water year, which is 34% ±12% of the precipitation (95% confidence). Soils on the southwest facing slope drain more often throughout the snow season, but the northeast facing slope contributes more total soil drainage for the water year. Peaks in catchment soil drainage and bedrock infiltration coincide with rain on snow events.

Introduction

Bedrock infiltration (BI) from mountain catchments, defined as water that leaves the catchment boundaries through subsurface drainage, is important from both catchment and groundwater perspectives. The typically thin soils in mountain catchments transmit water to the soil bedrock interface where water can travel laterally towards a stream or valley bottom, or infiltrate into underlying bedrock. From the catchment perspective, BI can be an important loss term in the water balance (Bales et al., 2011; Flerchinger and Cooley, 2000; Graham et al., 2010; Han et al., 2012; Kelleners et al., 2010). Small headwater catchments have been reported to lose up to 40% of annual precipitation to BI (Aishlin and McNamara, 2011), which can discharge down-gradient within larger catchments (Katsuyama et al., 2010) or enter regional groundwater systems (Thoma et al., 2011). The interaction of catchment surface water with bedrock groundwater can have significant controls on rainfall-runoff relationships (Katsuyama et al., 2010; Tromp-van Meerveld et al., 2007). From the groundwater perspective, BI can be an important source of mountain block recharge (Hogan et al., 2004; Thoma et al., 2011; Wilson and Guan, 2004). For example, most of the groundwater recharge in the Great Basin region occurs in the mountainous divides between basins (Flint et al., 2004; Hevesi et al., 2003; Scanlon et al., 2006). However, estimation of BI is difficult and hydrologic modeling studies often ignore this flux.

Quantifying the flux of water across the soil bedrock interface is challenging for many reasons. The hydraulic properties of bedrock are generally unknown, heterogeneous, and difficult to measure. The heterogeneity of overlying soils create variable propagation and storage of water in the soil profile even under uniform rainfall, and the soil bedrock interface may not be a sharp transition, but can be complicated by thick, variably weathered materials (e.g., saprolite). Although unique conditions may exist in some locations to allow direct measurement of BI, such as caves underlying catchments in karst terrain (Sheffer et al., 2011; Taucer et al., 2008), direct measurements are rarely possible due to the diffuse and inaccessible location of BI occurrence. Methods to quantify BI are generally indirect (Sammis et al., 1982) and include residual estimates from detailed mass balance studies of water or conservative solutes (Aishlin and McNamara, 2011; Graham et al., 2010), numerical modeling at a lower soil boundary (Dijksma et al., 2011; Guan et al., 2010; Kelleners et al., 2009; Kelleners et al., 2010; Selle et al., 2011; Wang et al., 2011), and using storage-discharge relationships (Ajami et al., 2011).

Annual mass balance approaches calculate BI as a residual, which includes the additive errors of all other mass balance components. Generally, these approaches cannot be used to assess the sub-annual timing of BI. Solute balance approaches also require multiple years of data to overcome inherent assumptions, and even then may only be correct when averaging over the period of record (Aishlin and McNamara, 2011; Wood, 1999). Numerical modeling of BI is hindered by a general lack of knowledge of the transmissive properties of underlying bedrock, which makes model parameterization challenging (Nolan et al., 2007; Sorensen et al., 2014; Sutanudjaja et al., 2011). Storage-discharge relationships (Brutsaert and Nieber, 1977; Kirchner, 2009) have been used to assess mountain block recharge by recognizing that changes in groundwater storage are related to both streamflow and recharge (Ajami et al., 2011). Inherent in this approach is the assumption that streamflow incorporates all drainage from catchment groundwater storage. In “leaky” catchments, however, streamflow does not represent all drainage. Rather, drainage is the sum of streamflow and BI. When BI is significant, traditional storage-discharge methods are not appropriate.

While many studies have estimated the magnitude of annual BI over catchments or regions (Jie et al., 2011; Ragab et al., 1997; Simmers, 1998; Van der Lee and Gehrels, 1997), few studies have estimated the timing of BI on sub annual timescales. The timing and magnitude of BI is complicated by rain on snow (ROS) events in the climatically sensitive rain snow transition zones of the mountainous western US. The rain snow transition zone is the elevation zone where the dominant winter precipitation phase changes from rain at lower elevations to snow at higher elevations. The elevation of this zone varies from sea level at high latitudes (Feiccabrino et al., 2012) to over 2000 m at lower latitudes (Cayan et al., 2001). This zone typically occurs between 1500 m and 1800 m in the interior Pacific Northwestern U.S. and covers approximately 9200 km^2 (Nolin and Daly, 2006). The dominant phase of precipitation in the rain snow transition zone is expected to change from snow to rain as climate warming trends continue (Cuo et al., 2011; Lutz et al., 2012; Mote et al., 2005; Nayak et al., 2010) and the incidence of winter ROS events is expected to increase (Lettenmaier and Gan, 1990). Although ROS events are known to generate large amounts of runoff (McCabe et al., 2007), there is a general lack of knowledge about how much BI they produce at event and annual timescales.

The goal of this study is to quantify the magnitude and sub-annual timing of BI in a semiarid mountain catchment in the rain snow transition zone north of Boise, Idaho, USA (**Figure 1**). A water balance approach at the soil bedrock interface is employed that assumes water draining to the soil bedrock interface, DR, is either routed laterally to streamflow, or vertically to bedrock infiltration. Drainage to the soil bedrock interface is modeled using a physically based distributed snow model (*Isnobal*) loosely coupled to a soil capacitance model (*SEM*). BI is then simply modeled drainage minus measured streamflow. Uncertainty estimates are also made for each all terms in the mass balance. This paper addresses the following questions: 1) What is the spatiotemporal distribution of DR to the soil bedrock interface, 2) What is the uncertainty in simulated BI using a storage-based model, 3) what is the magnitude and timing of BI in a rain snow transition zone catchment, and 4) what are the relative contributions of ROS, snowmelt, and other events to total annual BI.

Background

BI is investigated in a mountain catchment with thin soil and an intermittent stream by employing a water balance approach at the soil bedrock interface. While recognizing that the hydrologic pathways of water arriving at the soil bedrock interface are complicated, we assume flow arriving at this surface is partitioned either laterally into streamflow, or vertically into BI. Estimating BI is then a matter estimating flow to the soil bedrock interface, henceforth referred to as drainage (DR), and measuring streamflow. The former requires hydrologic modeling to bypass the insurmountable difficulties of measuring basin wide soil drainage.

We chose a modular hydrologic modeling approach that allowed us to apply detailed physically based distributed models for some essential processes while conceptualizing other processes with simple, more efficient approaches (e.g. Bartolini et al., 2011; Papalexiou et al., 2011; Zhang et al., 2008). This approach relies on site-specific knowledge of both the hydrologic processes that must be faithfully represented, as well as those that can be simplified. Previous work in the study site, the Dry Creek Experimental Watershed, has demonstrated the following principles that have guided our model development: (1) snow accumulation and melt patterns are highly variable in time and space (Anderson et al., 2014; Kormos et al., 2014a; Kormos et al., 2014b), (2) spatial variability of soil moisture is correlated with the spatial variability of snow cover and snow melt (Williams et al., 2009), (3) lateral flow in the unsaturated soil column and overland flow is negligible (McNamara et al., 2005), (4) spatial and temporal patterns in hillslope soil moisture are related to intermittent streamflow (McNamara et al., 2005), and (5) streamflow in upland intermittent streams is disconnected from deep, regional groundwater (Miller et al., 2008). We also recognize that catchment storage is central to hydrological processes on all scales and is becoming increasingly recognized as an important control on water flux thresholds, slope connectivity, and residence times (Kirchner, 2009; McNamara et al., 2011; Spence, 2007; Spence et al., 2010).

This previous work suggests that hydrologic fluxes in the study site are dependent on the spatial distribution of snow accumulation and melt, and the storage and transmission properties of soil. We therefore present a combined modeling and measurement study that focuses on catchment water storage in snow and soil reservoirs within the study catchment. We used the physically based *Isnobal* model to calculate surface water input (SWI), which is the sum of snowmelt, rainfall that drains through the snowpack, and rainfall on bare ground (Reba et al., 2011; Winstral and Marks, 2002). SWI output from *Isnobal* is used as a boundary condition for a hydrology model that simulates subsurface flow and storage processes. *Isnobal* has been successfully used to provide SWI to hydrologic models of differing complexity. In the Boise River basin (2150 km^2), *Isnobal* was coupled to a water balance and streamflow simulation model to demonstrate that a spatially distributed energy balance snowmelt model can be used in a large mountainous catchment using data from existing meteorological networks (Garen and Marks, 2005). In the Reynolds Mountain East subwatershed of the Reynolds Creek Experimental Watershed (0.39 km^2) in the Owyhee Mountains of southern Idaho, *Isnobal* was coupled to the more complex *PIHM* model to illustrate the consequences of using a temperature index snowmelt model compared to using physically based snowmelt model (Kumar et al., 2013). In the current study, we use the Soil Ecohydraulic Model (*SEM*), a soil water capacitance-based parametric model to estimate BI from the rain snow transition zone (Seyfried, 2003).

The combination of a detailed physically based model to provide simulated SWI to a conceptual soil model is similar to the approach used by Seyfried et al. (2009). Soil water dynamics in that study were simulated for wide range of soil and SWI conditions for 2 years in Reynolds Mountain East, which is known to have an extreme spatial range in SWI resulting from snow drifts (Marks and Winstral, 2001). The Seyfried et al. (2009) study: 1) verified that *Isnobal* calculated snow depth was accurately distributed in space and time across Reynolds Mountain East, 2) found close agreement between measured and SEM-simulated soil water content in 14 different soil profiles over a two year period, 3) demonstrated that a catchment-wide effective storage capacity could be determined from spatially distributed soil water dynamics, and 4) showed that catchment-wide soil water drainage through the root zone was in close agreement with measured streamflow. Reynolds Mountain East is underlain by volcanics, which allowed for rapid subsurface lateral flow in the bedrock, and a relatively impermeable discontinuity at the weir limiting BI. The lesson for this current study is that accounting for the timing of the one-dimensional delivery of water to the soil bedrock interface is more important than accounting for two-dimensional lateral fluxes. Because both BI and streamflow result from hydrologic partitioning at the soil bedrock interface, we argue that BI can also be also simulated well with this approach.

An important difference between the Seyfried et al. (2009) study and the current study is that the Treeline catchment is underlain by granite, where flow is assumed to be limited to fractures. This fracture flow makes it difficult to collect all water exiting the catchment via lateral flow at a weir, and makes flow at the soil bedrock interface important. Watershed hydrologists commonly assume that the flow collected at a mountain weir accounts for all flow from a catchment. However, the amount of flow that exits these basins by a combination of BI and fracture flow is generally unknown.

In this study, BI is simulated for the 2011 water year (WY2011), October 1, 2010 through September 30, 2011. SWI from the *Isnobal* model is obtained from Kormos et al. (2014a). Distributed point measurements of snow depth, snow density, and soil moisture are used to calibrate and validate modeled snow and soil storage results, in contrast with the more common approach of calibrating to streamflow. The flux of interest, BI, cannot be used for calibration as coincident validation data for BI are not available. Fortunately, other studies estimate BI in the highly instrumented Treeline catchment of the Dry Creek Experimental Watershed, henceforth called Treeline, (*referred to as Upper Dry Creek in* McNamara et al.,(2005)) using a variety of methods. Aishlin and McNamara (2011) estimate that Treeline loses between 17% and 44% of annual (wind-corrected) precipitation to BI using a chloride mass balance approach for 2005 through 2009. Kelleners et al. (2010) arrive at a similar conclusion (34-36% of measured shielded precipitation) by applying a physically based hydrology model to the catchment. In the latter study, BI is represented with a Darcian equation and a calibration objective function that combines soil moisture and streamflow to get an optimized vertical saturated hydraulic conductivity of the bedrock. This current study builds upon previous work in the catchment by accounting for wind redistribution of snow to improve simulations of SWI (Kormos et al., 2014b), and by using better soils information for improved storage estimates (Kormos et al., 2014a). By accounting for the snow and soil water dynamics that are important at this site, we are able to provide BI estimates at a sub-annual time scale. Additionally, we perform improved BI uncertainty estimates.

Study Site

Treeline is an intensively instrumented 1.5 ha catchment within the Dry Creek Experimental Watershed in the semiarid foothills north of Boise, ID (**Figure 1**). The catchment is defined by the location of a v-notch weir in the intermittent stream channel. Treeline ranges in elevation from 1600 m to 1645 m, which situates it in the current rain snow transition zone. It is dominated by northeast (NE) and southwest (SW) facing slopes. The catchment is underlain by fractured granitic bedrock (Gribb et al., 2009). Thin sandy soils range in thickness from 20 cm to 125 cm and average 48 cm (Williams et al., 2009). Soils are underlain by up to 100 cm of saprolite. Wet season conductive anomalies identified from an electrical resistivity tomography survey suggest water percolation through bedrock fractures (Miller et al., 2008). That survey and the intermittent behavior of the stream suggest a lack of connection between the stream and the regional groundwater storage reservoir. Vegetation is typical of a transition between lower elevation grasslands and higher elevation forests. The NE slope is typified by mountain big sagebrush and *ceanothus* shrubs, *prunus* subspecies, forbs, and grasses. SW slopes have sparser vegetation and contain mostly grasses, forbs, and sagebrush. There are 8 mature conifer trees in the catchment that are assumed to have negligible influence on the catchment hydrology for the purpose of this study.

The Treeline meteorological station has been operational since 1999. The average annual measured precipitation at the shielded gauge is approximately 670 mm with a mean annual temperature of 9°C. This study focuses on WY2011, which received above average precipitation totaling 855 mm measured at the shielded gauge, of which 43% of fell as snow, 49% fell as rain, and 8% fell as mixed events. The catchment experienced 2 major and 3 minor ROS events in WY2011. The 2011 snowpack was highly variable in time and space due predominantly to aspect differences in energy balance terms and wind redistribution of precipitation during snow storms (Kormos et al., 2014a; Kormos et al., 2014b). The mean WY2011 air temperature was cooler than average with a mean of 7.4°C.

Methods

Conceptual Approach

Whole catchment bedrock infiltration (BI_{WC}) is calculated as the residual of the catchment water balance integrated over a specific duration, T, as

$$BI_{WC} = \int_T [SWI_t - ET_t - Q_t - dS_t]dt \qquad (1)$$

where SWI_t, ET_t, Q_t, and dS_t are the magnitudes of whole catchment SWI, evapotranspiration, streamflow, and change in water storage, respectively, at time instant t. The terms SWI_t, ET_t, dS_t are combined to calculate whole catchment drainage, DR_t, which is the water that drains from the base of the soil profile to the soil bedrock interface

$$DR_t = SWI_t - ET_t - dS_t \qquad (2)$$

A premise of our approach is that water that drains to the soil bedrock interface is either routed laterally along the interface to the stream, or infiltrates into the bedrock and becomes BI. Thus, BI_{WC} is the difference between DR_t and Q_t integrated over T

$$BI_{WC} = \int_T [DR_t - Q_t] dt \quad (3)$$

This approach assumes that the lag time between DR_t and Q_t is negligible relative to T. Spatially, DR_t is represented as

$$DR_t = \frac{1}{A} \iint DR_{x,y} dxdy \quad (4)$$

where A is the catchment area, x and y are the coordinates of points in A, $DR_{x,y}$ is the drainage from the soil column at all such points at time t. Combing Equations 1, 3, and 4 yields

$$BI_{WC} = \int_T [(\frac{1}{A} \iint DR_{x,y} dxdy)_t - Q_t] dt \quad (5)$$

In this study, time in Equation 5 is discretized to daily time steps (t=1 day) so that

$$BI_{WC} = \sum_{t=tb}^{te} (DR_t - Q_t) \quad (6)$$

where tb and te are the beginning and ending days defining T, and DR_t and Q_t are catchment drainage and streamflow for each day, t. DR_t in Equation 6 is obtained by summing the drainage from Thiessen polygons surrounding all modeled points in a catchment at time t.

$$DR_t = \frac{1}{A} \sum_{p=1}^{P} DR_p A_p \quad (7)$$

where DR_p and A_p are the drainage and area of any given polygon, p, and P is the total number of polygons. In this study, we used 57 model points to create Thiessen polygons where soil depth and texture were measured (Williams et al., 2009)(**Figure 2**).

Substituting Equation 7 into Equation 6 yields a final equation for calculating BI_{WC} over any duration of interest using modeled DR_p and measured streamflow

$$BI_{WC} = \sum_{t=tb}^{te}[(\frac{1}{A}\sum_{p=1}^{P} DR_p A_p)_t - Q_t] \qquad (8)$$

Models

Drainage from each soil polygon is calculated according to Equation 2 using a storage-centric modeling approach similar to Seyfried et al. (2009). The *Isnobal* model, responsible for simulating SWI (Kormos et al., 2014b), and the Soil Ecohydraulic Model (*SEM*), responsible for simulating water draining from the soil column, are loosely coupled.

Isnobal

Details of the *Isnobal*-derived SWI time series used as the surface flux (Neumann boundary condition) to the soil surface layer can be found in (Kormos et al., 2014b). This study accounted for wind redistribution of snow, albedo decay from late season litter accumulation, and partial snow cover. *Isnobal* was run at an hourly time step on a 2.5 m^2 grid. This resulted in the hourly, distributed SWI to the catchment required to run the *SEM* model across the catchment. Since *SEM* was run at a daily time step at 57 points across the catchment, modeled SWI output was averaged spatially and accumulated temporally. To do this, the catchment was first divided into dominant slopes (**Figure 2**). The SW slope was divided into two dominant slopes so the differences in snow characteristics could be better translated to *SEM* polygons. This division is only used to create *SEM* domains and all results are grouped by NE and SW slopes. Thiessen polygons were then created within each slope to assign each of the 57 modeled points a catchment area. All pixels within each polygon were then averaged for each hourly time step and accumulated by day as input to *SEM*.

Soil Ecohydraulic Model (*SEM*)

SEM is a one-dimensional, soil water capacitance-based parametric model to estimate soil water storage, DR, and evapotranspiration (ET). It follows models developed by Hanks (1974), Wight and Hanks (1981), and Ritchie (1985) and is similar to that described by Evans et al. (1999) in that the approach focuses on soil water storage as opposed to calculating the flux through the soil. The model is described in somewhat different context in Seyfried et al. (2009); Seyfried (2003), and Finzel et al. (*in review*). *SEM* requires time series of SWI, minimum and maximum air temperature, and incoming shortwave radiation as boundary conditions (**Figure 3**). DR is calculated as the excess SWI after soil water storage and ET demands are met. *SEM* assumes water drains vertically downward through user-defined soil layers in accordance with parameters that describe the vegetation dynamics and soil properties (Seyfried, 2003; Seyfried et al., 2009). Soil layers are assigned hydraulic parameters describing water retention and drainage characteristic including soil saturation water content (*SAT*), field capacity (*FC*), and plant extraction limit (*PEL*) (Seyfried et al., 2009). Capacitance-based models rely on the concept that soils have a FC soil moisture content below which drainage due to gravity becomes negligible. Soil moisture excursions above FC provide water for DR and BI.

SEM assumes that there is no overland flow and all SWI infiltrates into the soil within each time step. *SEM* calculates water content for each soil layer at each time step. If SWI is greater than *SAT* of the top layer, the water content of the top layer is assigned to be equal to *SAT*, and additional water is routed to successively deeper layers. This process is repeated until all of the SWI is accounted for in the soil layers. If all layers are saturated, additional SWI routes directly to DR from the polygon, DR_p.

After the infiltrated water gets distributed among soil layers, water drains from each layer. The rate of water loss by drainage in the absence of additional inputs or outputs can be approximated as an exponential decline towards FC (Hillel, 1980). The exponential drainage assumption is based on the widespread observation that the rate of soil drainage is proportional to the amount of water stored in the profile above FC. Given this approximation, for any given soil layer the volumetric water content (θ) at the end of a time period is equal to

$$\theta = FC + (\theta_0 - FC) \times \exp\,(RDK \times \Delta t) \qquad (9)$$

where the subscript *0* represents the initial condition and Δt is the time interval the water balance is calculated over. The amount of water leaving a given soil layer, DR is

$$DR = (\theta_0 - \theta) \times \Delta z \qquad (10)$$

where Δz is the layer thickness. The rate that θ approaches FC depends on the value of the redistribution constant, RDK, is calculated as

$$RDK = \frac{\log(0.05)}{RDT} \tag{11}$$

where *RDT* is a redistribution time estimated as the length of time required for 95% of the soil water to drain. We used a suggested *RDT* value of 7.5 days (Seyfried et al., 2009) because it matched measured soil moisture responses to melt-drain events, where the soil wets quickly then drains in the absence of SWI or ET (**Figure 4**). *RDK* could also be calibrated to measured data, however, the *RDT* term gives an intuitive idea of how drainage occurs in soils. In the absence of ET and SWI, and as consecutive time steps reach *RDT*, θ will approach *FC*.

After soil drainage from each layer is calculated, ET is modeled within *SEM* using a modified Priestly-Taylor approach (Priestley and Taylor, 1972) when snow cover is gone from the surface. Since snow cover was modeled separately from *SEM*, the code was modified to accept a snow flag indicating the presence or absence of snow cover. Daily potential evapotranspiration (*PET*) is calculated by:

$$PET = 1.26 \times \left(\frac{\Delta}{\Delta + \gamma}\right) \times \frac{R_n}{\lambda_v} \tag{12}$$

where Δ is the slope of the saturated vapor pressure versus air temperature line, R_n is the average daily net radiation, λ_v is the latent heat of vaporization, and γ is the psychrometric constant (Arnold et al., 1990). R_n is calculated from average incoming shortwave radiation, a surface albedo, and average air temperature.

Actual evaporation from the soil surface (E) is calculated as a function of PET, the energy limitation provided by vegetative shading (E_{el}), and the time (days) from the most recent water input event (t_{swi}) such that:

$$E_{el} = PET \times \exp\,(-0.4 \times LAI_t \qquad (13)$$

and

$$E = E_{el} \times \left(\sqrt{t_{swi}} - \sqrt{t_{swi} - 1}\right) \qquad (14)$$

(Ritchie, 1979; Jenson et al., 1990). E_{el} proceeds to a user-defined minima (0.02 m^3 m^{-3}). Surface evaporation from under snow cover is assumed to be zero. E is bounded to have a maximum value of 2 mm on a day where SWI occurs.

Transpiration is dependent on the amount of exposed leaf area, which follows strong seasonal trends. The annual vegetative “green up” in the spring and “brown down” in summer, which are strongly driven by solar radiation and temperature due to a lack of summer rainfall, is represented by the following equation in which the constants C and D are empirical, LAI max is the maximum annual LAI, GS_{st} is the start of the growing season and GS_{pk} is the date of maximum LAI. See Seyfried (2003) for example applications.

$$LAI_t = LAI_{max} \times \left[\frac{t - GS_{st}}{GS_{pk} - GS_{st}}\right]^C \times exp\left(\frac{C}{D} \times 1 - \left[\frac{DOY - GS_{st}}{GS_{pk} - GS_{st}}\right]^D\right) \qquad (15)$$

The non-soil water limited potential transpiration ($PTran$) is calculated as:

$$PTran = \frac{PET \times LAI_t}{3} \quad (16)$$

Actual transpiration (*Atran*) is limited by the amount of plant available water in the wettest soil layer and ranges from *PTran* in wet soil to 0 at PEL such that:

$$ATran = Ptran \times maxratio \quad (17)$$

where *maxratio* is a measure of the water availability of wettest soil layer

$$maxratio = max\left(\frac{\theta_i - PEL_i}{FC_i - PEL_i}\right) \quad (18)$$

PTran is set to *PET* if LAI_t is greater than or equal to 3.0. The *i* subscript indicates the soil layer. *ATran* is distributed across soil layers based on a combined weighting function that accounts for the proportion of a layer of the total profile thickness, available soil moisture, and root distribution. The root distribution is assumed to have an exponential decline with depth based on a user-defined maximum rooting depth (Jackson et al., 1996). A constraint is imposed so that the sum of *P* and *E* cannot exceed *PET*.

Modeled soil water storage (S_t) at time *t* is calculated from modeled θ_i remaining after DR and ET are accounted for in all layers as:

$$S_t = \sum_{i=1}^{\#soil\ layers} \theta_i z_i \quad (19)$$

where z_i is the soil layer thickness of layer i. Measured S_t is calculated much the same way from measured θ from all depths in soil moisture profiles. Both field measurements and model outputs are expressed in θ_i and converted to storage to get a magnitude of water storage.

Parameterizing the Soil Ecohydraulic Model

Soil layers are defined for each of the 57 model points where soil depth (**Figure 2**) was measured based on the following criteria. Each point consists of a 2.5 cm soil surface layer that is underlain by a 7.5 cm layer. The thickness of deeper soil layers is dependent on measured soil depth at that location (Figure 2). If a soil profile is less than 30 cm, the rest of the soil depth is taken up with a third layer. If the soil profile is deeper than 30 cm, a third layer is assigned a thickness of 12.5 cm. If a soil profile is less than 60 cm, the fourth soil layer takes up the rest of the soil depth to bedrock. If the soil profile is greater than 60 cm, the fourth layer is 22.5 cm thick, and a fifth layer will take up the rest of the soil depth until a pit reaches 100 cm. If a soil profile has a depth over 100 cm, a 30 cm fifth layer is created and the rest of the soil depth is attributed to a sixth layer. The maximum number of soil layers used in this study is six. This scheme allows for a surface layer with large evaporative flux and close comparison between many of the measured and modeled soil moisture contents.

Model parameters required by *SEM* that were not directly measured are listed in **Table 1** with a brief description of the method used to obtain values. Values of *SAT*, *FC*, and *PEL* need to be provided for each soil layer. *FC* and *PEL* are empirically derived from measured soil moisture time series following the methods of Smith et al. (2011) (**Figure 4**). A separate linear relationship between soil depth and *FC* was developed for the NE and SW

(**Figure 5a and b**). Separate step models between soil depth and *PEL* values were developed for the NE and SW slopes (**Figure 5c and d**). A minimum *PEL* value of 0.040 was used for both slopes for soil depths between 0 cm and 5 cm. Soil layers on the NE slope with a midpoint deeper than 5 cm were assigned a *PEL* value of 0.093, while soil layers on the SW slope with a midpoint deeper than 5 cm were assigned a *PEL* value of 0.072. *SAT* was defined for all soil layers using an empirical relationship using soil texture (Flerchinger et al., 1996; Flerchinger and Pierson, 1991; Saxton et al., 1986). Measured surface soil texture data (0-30 cm) was used to calculate *SAT* for appropriate soil layers. Deeper soil texture values were obtained from sparse measurements on the north aspect (Yenko, 2003). A snow-free surface albedo of 0.15 was used based on 4-component radiometer data from the site, which agrees with albedo values used by Flerchinger et al. (1996) for a similar site.

Rooting depth was assumed to be the measured soil depth, which assumes that plants root to the bedrock surface. Previous studies (Spence, 1937) and field observations on the NE slope confirm the presence of roots at the bedrock surface. This assumption limits transpiration to the soil zone and disregards transpiration from the fractured bedrock zone. We acknowledge that roots may extend into the fracture network and there may be some transpiration from below the soil bedrock interface. However, we believe that the contribution is small because the storage capacity in the bedrock is small. This assumption appears reasonable in light of the relatively low stature, sparse vegetation on the site relative to the annual precipitation. That is, summer time transpiration is dependent on stored water, which appears to be very limited.

Separate LAI time series are constructed for *SEM* points on NE and SW slopes because of observed differences in vegetation. Three of the six parameters that define the LAI time series (Equation 15) were optimized to each slope using measured soil moisture between plant green up and soil dry down (April 5th, 2011 to July 20st, 2011)(**Table 2**). Prior knowledge of soil dynamics at Treeline leads us to use the snow meltout dates for the GS_{st}. Slope average meltout dates are obtained from *Isnobal* modeled pixels. Constant C and D shape factors are selected to insure that the LAI time series rises quickly and returns to minimum value by mid-August, as is observed at Treeline. GS_{pk}, LAI_{min}, and LAI_{max} parameters are optimized to each slope using a constrained nonlinear search function (simplex gradient) to minimize the root mean square error (RMSE) between modeled and measured soil moisture. Measured soil moisture at all depths from profiles Npit3 and Npit4 on the NE slope, and profiles SU10, SU5, and SU20 on the SW slope were used. Profile SD5 was emitted from the LAI parameter optimization because of suspected upslope contributions to deep soil moisture values, which are not accounted for in *SEM*.

Measured Data

Driving data used in the modeling process, and soil moisture, soil depth, and soil texture data that were used to parameterize *SEM* are described in detail in Kormos et al. (2014a). Air temperature and incoming shortwave radiation were measured hourly at the Treeline weather station and processed to daily values. Soil moisture data was collected at two soil moisture profiles, Pit3 and Pit4 installed on the northeast facing slope, and 5 soil moisture profiles, SD5, SU5, SU10, and SU20, installed on the southwest facing slope (Figure 1). Soil moisture instruments are either calibrated and temperature corrected water content reflectometers (Pit3 and Pit4), or time domain reflectometry probes (SD5, SU5, SU10, SU20), which are known to perform well in sandy soils (Chandler et al., 2004; Seyfried and Murdock, 2001; Topp et al., 1980). An existing overland flow collection plot on the NE slope was augmented with a lateral flow collection profile to quantify lateral water movement. A trench was dug to solid bedrock and grouted to inhibit vertical water loss. A pump was installed to move water from bedrock depressions to a tipping bucket when water was detected. Two steel collection troughs were installed at 125 cm and 40 cm below the ground surface in the trench face at soil boundaries, and water collected by these troughs were routed through tipping buckets. Snow data used to derive the modeled SWI time series include continuous snow depths from 6 sensors and 10 weekly repeated snow surveys, which consisted of distributed snow depth and density measurements.

Results

Surface Water Input

SWI modeling results from *Isnobal* are described in detail in Kormos et al. (2014b) and time series of slope average SWI and the timing of ROS events from this study are reproduced in **Figure 6a**. ROS events were delineated from the onset of atmospheric conditions associated with a rain event, which included increased air temperatures, wind speeds, and humidity, through the hydrograph recession associated with that event. Measured precipitation (779 mm unshielded, 855 mm shielded) was corrected for wind effects (935 mm) (Hanson et al., 2004), and snow storms were redistributed over the catchment (859 mm basin average) following a modified version of the methods presented by Winstral *et al.* (2013). This method calculated accumulation ratios for each model pixel based on slope breaks in the upwind direction, and the degree of sheltering from or exposure to wind from surrounding topography. Winter precipitation from October to

April was 35% rain, 10% mixed events, and 55% snow based on dew point temperatures (Marks et al., 2013). Modeled sublimation from the snowpack totaled 47 mm resulting in a basin average of 812 mm of SWI for WY2011. We estimated an uncertainty in total SWI of 32 mm based on the RMSE between measured and modeled snow water equivalent during 10 snow surveys (Kormos et al., 2014b). Uncertainty in the total precipitation amount due to wind redistribution alone was approximately +/-20 mm. We conservatively used the higher magnitude of 32 mm as our uncertainty in the SWI, since error in snow water equivalent is a combination of errors in accumulation, melt and sublimation (**Table 3**).

Streamflow (Q)

Q at Treeline typically initiates in the winter and ceases in the late spring to early summer (**Figure 7b**). During this study, streamflow initiated in mid-November. Due to equipment malfunction, continuous streamflow measurement began December 16th and continued through the cessation of flow in the summer. Early streamflow was gap filled using a series of 3 manual measurements and a multiple linear regression relationship between discharge at the TL weir and other nearby weirs within the larger Dry Creek Experimental Watershed (Kormos et al., 2014a). A total of 14 mm of streamflow was estimated, which is 4% of the total annual streamflow. Peaks in January, December, and March are associated with ROS events (**Figure 7b-c**). The total Q at the outlet weir for WY2011 was 325 mm (**Figure 6b**). We estimate the uncertainty in Q at 10% based on a lookup table category of "having a stable control structure with 8 to 12 stage-discharge measurements per year" (Harmel et al., 2006), and early season gap filling (**Table 3**).

Soil Moisture Observations and Simulations

The soil moisture time series for WY2011 illustrates the commonly observed behavior described by McNamara et al. (2005), with relatively stable wet and dry periods bounded by sharp increases and decreases (**Figure 4**). Soil moisture begins at the *PEL* in October and increases in response to fall rains and early snow accumulation-melt cycles. Deep soils on the NE slope generally reach *FC* in December in response to snowmelt and a ROS event. The soil moisture values remain at or above *FC* until early May, when elevated ET fluxes begin to dry the soil below *FC*. Spring rains extend the time that soil moisture is elevated above the *PEL*, which is reached between early July and mid-August.

Lateral flow occurs predominantly at the soil bedrock interface as deep soil moisture increases above approximately 0.20 m^3m^{-3} during the December ROS event (**Figure 8)**. This example time period is chosen because of suspected tipping bucket failure following this event. Overland flow data is not included because expected errors due to the area of the collection trough are an order of magnitude larger than the overland flow recorded. No lateral flow was collected at the trough approximately 125 cm below the soil surface.

Modeled shallow soil moisture commonly peaks higher and flatter than measured data on the NE slope. Modeled soil moisture at 15 cm repeatedly drops below measured data (**Figure 4**). Discrepancies between measured and modeled soil moisture are most likely a result from errors in the timing and magnitude of modeled SWI or mischaracterizing the soil parameters in *SEM*. The slower modeled soil moisture drawdown at 100cm is likely a result of the assumption that the root distribution declines exponentially with depth. High and flat modeled peak values may be an artifact of the daily time step used in *SEM*. Although it is clear that the daily time step used in the model does not accommodate large events, especially on moist soils, over longer time frames the net changes in storage are reasonably accurate.

The modeled storage from SEM19 fits measured data from SU5, SU10, and SU20 relatively well (**Figure 9**). Modeled storage from SEM8 performs well during wet-up when compared to measurements at both pits N3 and N4, but underestimates the storage from Npit3. These discrepancies demonstrate the high variability in soil moisture values measured over a relatively short distance. For comparison purposes only, the soil layer depths used to calculate modeled storage are combined to match the measured layer soil depths at the soil pits. This allows us to use the modeled soil moisture to calculate storage for thicknesses of soil at the measurement profiles for direct comparisons. Systematic deviations between measured and modeled soil water storage are attributed to uncertainty in the LAI time series, the distribution of *PEL* and *FC* soil parameters, or preferential flow, which allows deeper soils to wet up quickly. Area weighted RMSE between measured and modeled soil water storage for the 2 hillslopes is 19 mm.

The WY2011 total DR_t is 614 mm (**Figure 6b**). Cumulative DR from the SW slope was higher through most of the snow season. In late April, however, cumulative drainage from the NE aspect increased due to late-season snowmelt after the SW slope was snow-free.

Modeled Evapotranspiration

The WY2011 total modeled ET_t calculated was 196 mm (**Figure 7c**). Since ET is not directly measured, it is difficult to estimate the modeled ET_t error. However, we attempted to estimate the uncertainty in ET_t using a suite of model parameter sets that define the LAI time series. LAI time series parameter sets were obtained by separately calibrating to each soil moisture measurement profile (2 on the NE slope and 4 on the SW slope) during the time period when ET was active (April 5th to July 20th). Profile SD5 was excluded from the ET error analysis because of suspected upslope contributions to deep soil moisture, which is not accounted for in *SEM*. We then ran a Monte Carlo simulation, were every possible combination of parameters sets for the 2 slopes were used to run *SEM* distributed across Treeline. The standard deviation in the total modeled ET_t from these runs was 6 mm. We acknowledge that this method addresses the uncertainty in model parameters and does not address the uncertainty in ET_t due to model structure, which we do not have sufficient data to address. However, *SEM* has been shown to perform well during the late spring and summer, when ET is the dominant soil water flux, in watersheds with similar vegetation and soil depths, (Seyfried, et al., 2009). For the purpose of this study, we assume that there is no error in ET_t due to model structure.

Bedrock infiltration in the Annual Water Balance

BI_{WC} is estimated from Equation 8 as 289 mm, which is 34% of the basin-averaged distributed precipitation. The uncertainty associated with this BI estimate cannot be obtained by comparing it to direct measurements. We can, however, obtain a combined uncertainty in total WY2011 BI_{WC} from estimated uncertainty in total Q_t, SWI_t, ET_t and dS_t. Uncertainty in SWI_t and dS_t are obtained by comparing measured and modeled results, uncertainty in Q_t are obtained by best practices (Harmel, 2006), and uncertainty in ET_t are obtained by Monte Carlo techniques (**Table 3**). If the errors in modeled SWI_t, dS_t, ET_t, and measured Q_t are assumed to be normally distributed and uncorrelated, a simplified error propagation equation (resulting error is the square root of the sum of the squares) can be used to estimate the error in BI_{WC} for the WY2011 as 50 mm. This coincides with 34% ±12% of the distributed precipitation at 95% confidence and 34%±6% at 68% confidence using the standard deviation of the simulations. We also note that this estimate does not include instrument error or spatial correlation.

However, the assumption that errors in SWI_t, dS_t, and ET_t are not correlated, which allows us to overlook cross correlation terms in the error propagation equation, varies in strength according to the state of the snowpack, ET activity, and the soil storage state. Although errors in measured Q_t are likely weakly correlated to other errors, SWI_t, dS_t, and ET_t are mathematically related in the model. The assumption that errors in these variables are uncorrelated is strong at the beginning and end of the water year, when soil moisture is at PEL and there is little SWI. Although there is correlation between variables during wet-stable periods, the absence of significant ET and DR will minimize errors to BI_{WC}.

The assumption that errors are not correlated during the time period from April 7th (snow meltout date for south slope) to July 1st (Q_t is zero and soil moisture is well below FC), when ET is active, there is SWI, and soil is actively draining, requires more substantiation. This time period has the highest potential for creating errors in water year estimates of BI_{WC} since ET and DR processes are occurring simultaneously. For a water year estimate of BI, correlations between SWI_t, dS_t, and ET_t are only important when an error in SWI_t causes change in an error in ET_t via changes in dS_t. Although SWI_t and dS_t errors are highly correlated during this time (correlation coefficient = 0.98 at NE pits), errors in ET_t are negligibly correlated to errors in dS_t. This is because, following Equations 17 and 18, ET_t is not soil moisture limited during this time. Simulated soil moisture on the NE slope only briefly dips below FC. Further, during the summer dry down, there is no modeled drainage once soil moisture falls below FC. The only additional error that could be incurred due to correlation of errors would be if errors in SWI_t change either the amount of time that the wettest soil layer is below FC, or the magnitude of the soil moisture decline below FC. Since SWI_t is measured rain opposed to modeled snowmelt during this time, errors in that term will be minimal. In addition, ET_t values tend to be low surrounding times with precipitation since they tend to be cloudy and have high relative humidity.

Timing and Spatial Distribution of Soil Drainage (DR) and Bedrock Infiltration (BI)

SW slopes contribute to catchment DR more often than NE slopes from November to mid-January and also in late February due to a combination higher SWI and shallower soils (**Figure 2, 6b-c, and 10b-f**) (Kormos et al., 2014a; Kormos et al., 2014b). The magnitude of DR is also often higher on the SW slope until mid-March, after which the NE slope contributes more DR until early May. The SW slope DR increases more rapidly in response to precipitation and melt events from the onset of streamflow in early December to mid-March (**Figure 6c**). This is a result of a more limited storage capacity (shallower soil depth) on SW slopes (Smith et al., 2011). NE slope DR peaks higher and remains elevated longer staring mid-March (**Figure 6c**). The SW slope contributes more cumulative DR until the beginning of April, just after the final spring melt commences (**Figure 6b and 11**). The NE slope contributes more DR per area by the end of WY2011, mainly as a result of winter precipitation distribution (Kormos et al., 2014b).

Although we can comment on the spatial distribution of DR, it is difficult to translate that knowledge to a spatial distribution of BI because of lateral flow at the soil bedrock interface and the unknown transmissive properties of that interface. The timing of

BI peaks coincides with peaks in modeled whole catchment soil storage as well as peaks in measured Q_t (**Figure 7**). Negative BI calculations are a result of measured Q_t being greater than modeled DR_t, which occurs when Q_t increases before DR_t (December 14th), Q_t peaks higher than DR_t (March 16th), or the Q_t recession is slower than the DR_t recession. Negative BI values are simply a modeling artifact and do not infer exfiltration of water from the bedrock. Faster measured Q_t increases may be a result of 1) quick flow paths that are active in Treeline, but not accounted for in the model, such as lateral flow within the snowpack (Eiriksson et al., 2013), overland flow, or macropore flow, 2) faster soil water redistribution in Treeline compared to the modeled soil water redistribution, or 3) errors in the timing of SWI calculations from *Isnobal*. Slower Q_t recessions occur when modeled DR_t reaches a zero value quickly after SWI events, while measured streamflow recedes slower. The prolonged measured streamflow recession is evidence that there is certainly a time lag associated with lateral flow in Treeline. This is a result of lateral flow from the area of DR taking some amount of time to get to the stream outlet. If this time lag is greater than the model time step (1 day), it will lead to errors in Equation 2 when creating a BI time series (**Figure 7c**). We assume negative BI values do not affect qualitative conclusions about the timing of BI events at time scales greater than 1 day. Negative estimates of daily BI values from May 2nd to July 1st result from Q_t recession being slower than DR_t recession. Discharge measured in May could have entered the basin at any previous time step. The discussion of the timing of BI is therefore based on the additional assumption that these errors are distributed evenly across the water year. We can then quantify the relative importance of hydrologic in terms of BI. ROS events from December, January, and March contribute 17% of BI, while the spring melt event on the NE slope contributed 31%.

Discussion

Soil Drainage and Bedrock Infiltration

BI was a large component of the annual water budget in WY2011 at Treeline. Drainage to the soil bedrock interface occurs from late October to June (**Figure 6c and 7b**). This is in contrast to higher elevation sites where DR is expected to occur only during the spring ablation season (Murray and Buttle, 2005; Seyfried et al., 2009). This mid elevation zone also receives greater amounts of precipitation than rain-dominated, lower elevations because of well-known orographic relationships. The timing and magnitude of DR from the rain snow transition zone may make it an important source of down slope, cold season streamflow (Knowles and Cayan, 2004). The timing of BI lines up with peaks in modeled whole catchment soil storage, as well as peaks in measured streamflow (**Figures 7**). Large BI events coincide with ROS events in mid-December, mid-January, and mid-March. The December ROS event began on December 11th and extended to December 19th. Estimated streamflow for this period rises earlier than modeled DR, causing a negative spike in BI. This may be a result of the gap filling methods used to estimate early streamflow (Kormos et al., 2014a). The January ROS event begins on January 12th and extends through January 20th. It also contains a large negative dip in the BI record on January 17th. This is primarily a result of modeled DR peaks not matching measured Q_s (**Figure 7b inset**), which may result from errors in modeled SWI or *SEM* model parameters. A ROS event occurring between March 12th and March 20th also includes a large negative dip because the DR and measured streamflow peaks are offset. Although 3 ROS events occur in April, they coincide with the spring snowmelt event on the NE slope (March 29th to May 1st). It is difficult to separate BI related to ROS events versus ongoing snowmelt.

Performance of storage-based modeling

Lateral flow at Treeline occurs primarily at the soil bedrock interface with little to no flow collected at the soil surface or soil horizons (**Figure 8**). This agrees with previous studies by Graham et al. (2010). We feel that this data is sufficient to justify the use of simplified modeling methods, including the use of a one dimensional model with vertical flow assumptions through the soil profile. The *SEM* model assumes that lateral moisture redistribution, such as overland flow or lateral flow in the soil column, is negligible. The existence of streamflow, however, implies that lateral redistribution does indeed occur. Implicit in our approach is the assumption that both BI_{WC} and Q_t result from partitioning of vertical infiltration at the soil bedrock interface. While some lateral redistribution of water likely occurs throughout the snow-soil bedrock profile, close agreement of measured and modeled soil storage (**Figure 9**), and modeled DR_t and measured Q_t (**Figure 7**) suggest that the magnitudes of lateral fluxes are small. Further, if such lateral fluxes reach the stream, they are incorporated into the total water year estimation of BI.

In the context of hydrologic modeling methods, the capacitance parameter approach approximates the process of redistribution (drainage) using parameters that are: 1) of relatively low spatial variability, 2) easily verified empirically, and 3) easily assessed in terms of impact of estimation error (if *FC* is 0.01 high, then simulated soil moisture will tend to be 0.01 high during the winter months). The focus on what is retained in the soil, as opposed to the soil water flux, has the advantage that no characterization of macropores is needed because *RDK* accounts for both Darcian and preferred flow soil drainage processes. This approach also takes advantage of the empirically observed thresholds in measured water contents corresponding conceptually to FC and PEL generally observed in soil water data measured the region (e.g., Seyfried et al., 2009; McNamara et al., 2005; Seyfried, 2011).

FC was initially defined as "the amount of water held in the soil after the excess gravitational water has drained away and after the rate of downward movement of water has materially decreased" (Veihmeyer and Hendrickson, 1931). The concept of FC has been widely criticized partly because it is not appropriate for many field conditions, such as where ground water influences water contents, and partly because the values determined from standard laboratory soil water potential values often do not match observations in the field (Hillel, 1998; Assouline and Or, 2014). Although the concept of FC can be ambiguous, it works well in our study area where DR and ET seasons are fairly distinct (McNamara et al., 2005), and field-measured values are used (e.g., Seyfried, 2011, Ladson, 2006; Ritchie, 1981). The approach has the advantages that it directly uses measured soil water content data, which are extrapolated using soil texture information. Soil texture is widely available and closely related to soil water retention and of only moderate spatial variability.

The capacitance parameter approach also avoids "physically based" parameters becoming "knobs" for tuning over parameterized models partly because they are so variable in space and difficult to verify empirically. A physically based Richards equation approach is often preferred for calculating soil water flux because it directly simulates the processes known to universally drive soil water movement. While this approach is clearly preferred for conceptual reasons, and where soil properties are well characterized, there are serious practical issues associated with most extensive field applications. With the Richards equation, movement of soil water is driven by the soil hydraulic potential gradient

(h) as modified by the hydraulic conductivity (K). Two functions, θ(h) and K(θ) are required. The θ(h) function is rarely measured in the field and generally estimated using pedotransfer functions that generalize over many soils but are rarely verified on site and subject to substantial error (e.g. Saxton and Rawls, 2006; Warrick and Nielsen, 1980). The K(θ) function is almost never measured in the field and is also estimated using pedotransfer functions that are largely based on soil texture. The function is strongly non linear and generally scaled to saturated hydraulic conductivity (K_{sat}), which is often measured in the field though usually only near the soil surface. Unfortunately, K(θ) spatial variability is extremely high and K_{sat} is poorly correlated with soil texture (Kutilek and Nielsen, 1994) leading to unknown but extremely high (orders of magnitude) estimation errors. The hydraulic potential gradient is rarely measured and of unknown variability but also contributes to the largely unknowable estimation error. These issues are generally addressed by calibrating various nonlinear parameters describing the functions. Thus, for extensive field applications, the problem is that soil water flux is calculated using unknown gradients modified by poorly estimated functions using an overparmeterized model (Beven, 1989).

We can directly compare our BI estimates to a chloride mass balance estimate made at Treeline for WY2011 using the same basin averaged distributed precipitation record used in this paper (unpublished data following Aishlin and McNamara (2011)). This approach estimates BI was 18% of precipitation of with a range from 3% to 37%, which is within the range of our estimate of 34%±12%. Our estimate may be in the upper range of the chloride mass balance estimate because of chloride flushing caused by midwinter ROS events. These events may have sufficient soil water fluxes to flush chloride ions from previous years through the soil profile. We additionally estimate the error in total WY2011 DR_t as the combined error in SWI_t, ET_t, and dS_t resulting in 614 ±38mm (Equation 2)(**Table 3**).

We cannot directly compare the BI estimate obtained in this paper to previous published estimates because previous estimates did not distribute snow storms based on wind. There was a difference of 76 mm between the wind-corrected and basin-averaged redistributed precipitation for WY2011 at Treeline. However, if we assume that the fraction of precipitation that BI accounts for is similar independent of the precipitation correction method, our estimate of 34% ±12% (basin- averaged, distributed) is within the estimates of 17 to 44% (wind-corrected) and 34% to 36% (measured shielded) from Aishlin and McNamara (2011), and Kelleners et al. (2010), respectively.

The similarity between our results and results obtained using other methods suggest that the storage-centric approach presented in this paper is a useful tool when streamflow is an unreliable calibration target due to BI. By focusing on simulating distributed soil moisture dynamics, we are able to estimate DR, which includes BI and Q_t. However, the method has several assumptions and drawbacks outlined in the following paragraphs that must be addressed.

The dominant storage reservoirs must be known and well characterized. Treeline is small and previous work demonstrated that snow and soil moisture storage dominate catchment response (Williams et al., 2009), while deep saturated groundwater flow is not important. As catchment size increases, storage mechanisms will likely become more complex and an appropriate subsurface model should be incorporated. Distributed SWI must be well characterized because this approach relies on estimates of distributed soil moisture storage and drainage. This is challenging in snow dominated catchments, necessitating physically based models driven by distributed inputs. The distribution of inputs is often difficult to obtain. In this study, precipitation was distributed according to empirical methods following Winstral et al. (2013) as described in Kormos et al. (2014b). The total amount of precipitation received by the catchment is sensitive to the parameters used in the wind redistribution procedure. An extensive dataset, including 10 repeat snow surveys and 6 ultrasonic depth sensors, was used to optimize these parameters. A minimum RMSE of 32 mm between measured and modeled snow water equivalent was obtained with the best parameter set.

Characterizing the soil and plant properties of a basin from point measurements is difficult given the high spatial variability involved. *FC* and *PEL* parameters are empirically obtained from 20 soil moisture probes and at various locations and depths in a 1.5 ha catchment. *SAT* parameter values were calculated from soil texture data obtained from the 57 model point locations. Even though this is a high density of measured data, we recognize that soil properties and soil moisture magnitudes are highly variable over short distances (Brocca et al., 2012; Fiener et al., 2012). Also, the placement of soil moisture probes on the SW slope is not ideal for calculating measured soil moisture storage. Shallow probes placed in the top 15 cm of the soil profile may be influenced by evaporation from the soil surface when the snow disappears, causing lower soil moisture contents in late March, even though *PET* is low. Deep probes were placed at the soil-saprolite interface and may measure soil moisture increased due to the collection of water at that interface instead of a lower value if the soil column was allowed to drain freely. Deep probes may also record prolonged elevated moisture because of the influence of lateral flow from upslope contributing areas. The location of the deep probes and the fact that there are only two probes in each pit (the deep probe represents less than 50% of the calculated soil storage value) may explain differences in measured and modeled soil water contents.

Aspect differences in soil and vegetation are considered a fundamental control on the hydrology of the study area (Geroy et al., 2011; Kunkel et al., 2011; Smith et al., 2011; Tesfa et al., 2009). Vegetation differences are accounted for in *SEM* by separate LAI time series for NE and SW slopes. SW slopes have shallower soil and abundant shrubs that are able to root well below the measured soil depth. Calibrated LAI time series for the NE and SW slopes generally agree with vegetation studies in similar areas (Clark and Seyfried, 2001; Flanagan et al., 2002; Flerchinger et al., 1996; Griffith et al., 2010; Groeneveld, 1997; Ivans et al., 2006; Steinwand et al., 2006). The LAI_{max} values are somewhat high for both the NE and SW slopes compared values reported in the literature. The high LAI_{max} values may be a result of a tree adjacent to the north soil pits and the fact that some south soil pits are close to the valley bottom where vegetation has access to water from the drainage network. Regardless of the high LAI_{max} values, the modeled soil dry down agrees fairly well with measured dry down where measured (**Figure 4 and 9**). Aspect associated soil differences are accounted for in this study by having separate *FC* and *PEL* relationships with soil depth for each aspect, varying *SAT* with texture data obtained from each aspect, and having measured soil depths across the catchment.

One of the main drawbacks of utilizing the modeled DR is that ET errors are inherited to BI (Essery and Wilcock, 1990; Scanlon et al., 2002; Simmers, 1998). ET can be an especially large term in semi-arid environments. *SEM* uses a modified Priestly-Taylor (1972) equation that incorporates time-varying LAI (Equation 11) (Rose, 1984; Seyfried,

2003) and available soil moisture (Shuttleworth and Maidment, 1992). Potential errors are assumed to be low in the winter, when temperatures are low and snow cover inhibits significant ET. Errors are expected to increase for much of April, when the soil moisture content is above *FC* (**Figure 4 and 9**), snow cover is absent (**Figure 3a**), and modeled ET is increasing (**Figure 7c**) (Blankinship and Hart, 2012; Krestovskiy et al., 1979; Willmott et al., 1985).

Conclusions

Bedrock infiltration from Treeline for the WY2011 is estimated as 298 mm ±50 mm or 34% ±12% of catchment average distributed precipitation. Both ROS and the spring melt contribute significantly to the total BI for WY2011. Large BI events coincide with ROS events in mid-December, mid-January, and mid-March. The SW slope drains more often throughout WY2011, but the NE slope contributes a greater total magnitude of DR.

The widely applicable modeling approach for estimating BI described in this paper focuses on a high degrees of similarity between measured and modeled soil water storage. The choice of hydrologic model or models used to distribute SWI and account for subsurface dynamics needs to be well suited to the specific study site. In this study, using loosely coupling *Isnobal* and *SEM* worked well at Treeline. Complex snow accumulation and melt dynamics warrant the use of a distributed physically based snow model, while relatively simple catchment soil properties allow us to use a capacitance based soil model to represent catchment soil dynamics. The agreement between the timing of measured discharge peaks and modeled soil outflow peaks is verification that the model performs well. The benefits of using *SEM* include a limited number of conceptually-tangible parameters leading to a relatively quick setup time and limited computational expense. However, these models, which neglect the time lag from soil drainage to streamflow, are expected to lead to degraded performance with increasing catchment size. The simplified approach described here may provide a good estimate of the timing and magnitude of recharge events at larger scales. Recharge estimates for larger basins with regional groundwater influences should consider a more complex model that represents the important hydrologic processes of that basin.

Notation

Units: l – length; t – time; m – mass; K – temperature; e - energy

A	catchment area (l^2)
A_p	area of polygon p (l^2)
$ATran$	actual transpiration (l)
BI_{WC}	whole catchment bedrock infiltration (l)
C	LAI shape factor 1 (unitless)
D	LAI shape factor 2 (unitless)
DOY	day of year at time t (unitless)
DR	drainage from the bottom of a soil layer (l)
DR_p	drainage to the soil bedrock interface from polygon p (l)
DR_t	whole catchment drainage to the soil bedrock interface at time t (l)
$DR_{x,y}$	drainage to the soil bedrock interface at location x,y at time t (l)
dS_t	whole catchment change is soil water storage at time t (l)
E	evaporation (l)
E_{el}	energy limited soil evaporation (l)
ET_t	whole catchment evapotranspiration at time t (l)
FC_i	field capacity of soil layer i ($l^3\ l^{-3}$)
GS_{pk}	day of year of peak growing season when LAI_{max} occurs (unitless)
GS_{st}	growing season start day of year (unitless)
LAI_{max}	maximum leaf area index ($l^2\ l^{-2}$)
LAI_t	leaf area index at time t ($l^2\ l^{-2}$)
$maxratio$	water availability of the wettest soil layer (unitless)
p	index for polygon summation (unitless)
P	total number of Thiessen Polygons in the catchment (unitless)
PEL	plant extraction limit ($l^3\ l^{-3}$)
PET	potential evapotranspiration (l)
$PTran$	potential transpiration (l)
Q_t	stream discharge at time t (l)
R_n	average daily net radiation ($e\ l^{-2}\ t^{-1}$)
RDK	soil water redistribution constant (t^{-1})

RDT	soil water redistribution time (t)
S_t	soil water storage (l)
SWI_t	whole catchment surface water input at time t (l)
T	time duration to be integrated over (t)
t_b	beginning time step of summation (unitless)
t_e	ending time step of summation (unitless)
t_{swi}	time from last water input event (unitless)
Δ	slope of the saturated vapor pressure vs. air temperature line (m l^{-1} t^{-2} K^{-1})
Δt	time interval for soil water balance calculation (t)
Δz	soil layer thickness (l)
z_i	thickness of soil layer i (l)
γ	psychrometric constant (m l^{-1} t^{-2} K^{-1})
λ_v	latent heat of vaporization (e m^{-1})
θ	volumetric soil water content at the end of the time interval Δt (l^3 l^{-3})
θ_i	volumetric soil water content of soil layer i (l^3 l^{-3})
θ_0	initial volumetric soil water content at the time interval Δt (l^3 l^{-3})

Acknowledgements

We thank Jason Williams and Seth Wenger for assisting in the preparation of this manuscript and Pam Aishlin for field data collection and processing. We thank the students, faculty, and scientists at the Northwest Watershed Research Center, Boise Aquatics Science Laboratory, and Boise State University Department of Geosciences for intellectual support. We thank the Northwest Watershed Research Center and Boise State University Department of Geosciences, Student Research Initiative, and Graduate College for funding support, travel support, and general support. NASA EPSCoR and INRA provided funding for this project. The collection and processing of the data presented in this paper were funded in part by NSF-CBET (0854553, 08522), USDA-ARS CRIS Snow and Hydrologic Processes in the Intermountain West (5362-13610-008-00D), USDA-NRCS Water and Climate Center-Portland, Oregon (5362-13610-008-03R), NSF-EPS (0919514), and NOAA (NA08NWS4620047). Any reference to specific equipment types or manufacturers is for information purposes and does not represent a product endorsement or recommendation. Boise State University and the USDA ARS are equal opportunity employers.

References Cited

Aishlin, P., McNamara, J.P., 2011. Bedrock infiltration and mountain block recharge accounting using chloride mass balance. Hydrological Processes, 25(12): 1934-1948, doi: 10.1002/hyp.7950.

Ajami, H., Troch, P.A., Maddock, T., Meixner, T., Eastoe, C., 2011. Quantifying mountain block recharge by means of catchment-scale storage-discharge relationships. Water Resources Research, 47(4), doi: 10.1029/2010WR009598.

Anderson, B.T., McNamara, J.P., Marshall, H.P., Flores, A.N., 2014. Insights into the physical processes controlling correlations between snow distribution and terrain properties. Water Resources Research, doi: 10.1002/2013WR013714.

Arnold, J.G., Williams, J., Nicks, A., Sammons, N., 1990. SWRRB; a basin scale simulation model for soil and water resources management. Texas A & M University Press, ISBN: 0-89096-337-1.

Assouline, S., Or, D., 2014. The concept of field capacity revisited: Defining intrinsic static and dynamic criteria for soil internal drainage dynamics. Water Resources Research 50(6): 4787-4802, doi:10.1002/2014WR015475.

Bales, R.C. et al., 2011. Soil moisture response to snowmelt and rainfall in a Sierra Nevada mixed-conifer forest. Vadose Zone Journal, 10(3): 786-799, doi: 10.2136/vzj2011.0001.

Bartolini, E., Allamano, P., Laio, F., Claps, P., 2011. Runoff regime estimation at high-elevation sites: a parsimonious water balance approach. Hydrology and Earth System Sciences Discussions, 8(1): 957-990, doi: 10.5194/hessd-8-957-2011.

Beven, K. 1989. Changing ideas in hydrology-the case of physically based models. Journal of Hydrology, 105(1): 157-172, doi: 10.1016/0022-1694(89)90101-7.

Blankinship, J.C., Hart, S.C., 2012. Consequences of manipulated snow cover on soil gaseous emission and N retention in the growing season: a meta-analysis. Ecosphere, 3(1): art1, doi: 10.1890/ES11-00225.1.

Brocca, L., Tullo, T., Melone, F., Moramarco, T., Morbidelli, R., 2012. Catchment scale soil moisture spatial–temporal variability. Journal of hydrology, 422: 63-75, doi: 10.1016/j.jhydrol.2011.12.039.

Brutsaert, W., Nieber, J.L., 1977. Regionalized drought flow hydrographs from a mature glaciated plateau. Water Resources Research, 13(3): 637-643, doi: 10.1029/WR013i003p00637.

Cayan, D.R., Dettinger, M.D., Kammerdiener, S.A., Caprio, J.M., Peterson, D.H., 2001. Changes in the onset of spring in the western United States. Bulletin of the American Meteorological Society, 82(3): 399-415, doi: 10.1175/1520-0477(2001)082<0399:CITOOS>2.3.CO;2.

Chandler, D., Seyfried, M., Murdock, M., McNamara, J., 2004. Field calibration of water content reflectometers. Soil Science Society of America Journal, 68(5): 1501-1507, doi: 10.2136/sssaj2004.1501.

Clark, P.E., Seyfried, M.S., 2001. Point sampling for leaf area index in sagebrush steppe communities. Journal of range management: 589-594, Stable URL: http://www.jstor.org/stable/4003589.

Cuo, L. et al., 2011. Effects of mid-twenty-first century climate and land cover change on the hydrology of the Puget Sound basin, Washington. Hydrological Processes, 25(11): 1729-1753, doi: 10.1002/hyp.7932.

Dijksma, R., Brooks, E.S., Boll, J., 2011. Groundwater recharge in Pleistocene sediments overlying basalt aquifers in the Palouse Basin, USA: modeling of distributed recharge potential and identification of water pathways. Hydrogeology Journal, 19(2): 489-500, doi: 10.1007/s10040-010-0695-9.

Essery, C.I., Wilcock, D.N., 1990. Checks on the measurement of potential evapotranspiration using water balance data and independent measures of groundwater recharge. Journal of hydrology, 120(1): 51-64, doi: 10.1016/0022-1694(90)90141-J.

Evans, S.P., Mayr, T.R., Hollis, J.M., Brown, D.C., 1999. SWBCM: a soil water balance capacity model for environmental applications in the UK. Ecological Modelling, 121(1): 17-49, doi: 10.1016/S0304-3800(99)00068-X.

Feiccabrino, J., Lundberg, A., Gustafsson, D., 2012. Improving surface-based precipitation phase determination through air mass boundary identification. Hydrology Research, 43(3): 179-191, doi: 10.2166/nh.2012.060.

Fiener, P., Dlugoß, V., Korres, W., Schneider, K., 2012. Spatial variability of soil respiration in a small agricultural watershed—Are patterns of soil redistribution important? Catena, 94: 3-16, doi: 10.1016/j.catena.2011.05.014.

Finzel, J.A., Seyfried, M.S., Weltz, M.A., Launchbaugh, K.L., *in review*. Simulation of long-term soil water dynamics at Reynolds Creek, Idaho: Implications for Rangeland Productivity, Ecohydrology.

Flanagan, L.B., Wever, L.A., Carlson, P.J., 2002. Seasonal and interannual variation in carbon dioxide exchange and carbon balance in a northern temperate grassland. Global Change Biology, 8(7): 599-615, doi: 10.1046/j.1365-2486.2002.00491.x.

Flerchinger, G., Cooley, K.-R., 2000. A ten-year water balance of a mountainous semi-arid watershed. Journal of Hydrology, 237(1): 86-99, doi: 10.1016/S0022-1694(00)00299-7.

Flerchinger, G., Hanson, C., Wight, J., 1996. Modeling evapotranspiration and surface energy budgets across a watershed. Water Resources Research, 32(8): 2539-2548, doi: 10.1029/96wr01240.

Flerchinger, G., Pierson, F., 1991. Modeling plant canopy effects on variability of soil temperature and water. Agricultural and Forest Meteorology, 56(3): 227-246, doi: 10.1016/0168-1923(91)90093-6.

Flint, A.L., Flint, L.E., Hevesi, J.A., Blainey, J.B., 2004. Fundamental concepts of recharge in the Desert Southwest: a regional modeling perspective. Groundwater Recharge in a Desert Environment: The Southwestern United States: 159-184, doi: 10.1029/009WSA10.

Garen, D.C., Marks, D., 2005. Spatially distributed energy balance snowmelt modelling in a mountainous river basin: estimation of meteorological inputs and verification of model results. Journal of Hydrology, 315(1-4): 126-153, doi: 10.1016/j.jhydrol.2005.03.026.

Geroy, I.J. et al., 2011. Aspect influences on soil water retention and storage. Hydrological Processes, 25(25): 3836-3842, doi: 10.1002/hyp.8281.

Graham, C.B., Van Verseveld, W., Barnard, H.R., McDonnell, J.J., 2010. Estimating the deep seepage component of the hillslope and catchment water balance within a measurement uncertainty framework. Hydrological processes, 24(25): 3631-3647, doi: 10.1002/hyp.7788.

Gribb, M.M., Forkutsa, I., Hansen, A., Chandler, D.G., McNamara, J.P., 2009. The Effect of Various Soil Hydraulic Property Estimates on Soil Moisture Simulations. Vadose Zone Journal, 8(2): 321-331, doi: 10.2136/vzj2008.0088.

Griffith, A.B., Alpert, H., Loik, M.E., 2010. Predicting shrub ecophysiology in the Great Basin Desert using spectral indices. Journal of arid environments, 74(3): 315-326, doi: 10.1016/j.jaridenv.2009.09.002.

Groeneveld, D.P., 1997. Vertical point quadrat sampling and an extinction factor to calculate leaf area index. Journal of arid environments, 36(3): 475-485, doi: 10.1006/jare.1996.0213.

Guan, H., Simunek, J., Newman, B.D., Wilson, J.L., 2010. Modelling investigation of water partitioning at a semiarid ponderosa pine hillslope. Hydrological processes, 24(9): 1095-1105, doi: 10.1002/hyp.7571.

Hanks, R.J., 1974. Model for prediciting plant yield as influenced by water use. Agronomy Journal, 66(5): 660-665, doi: 10.2134/agronj1974.00021962006600050017x.

Han, S., Yang, Y., Fan, T., Xiao, D., Moiwo, J.P., 2012. Precipitation-runoff processes in Shimen hillslope micro-catchment of Taihang Mountain, north China. Hydrological Processes, 26(9): 1332-1341, doi: 10.1002/hyp.8233.

Hanson, C.L., Pierson, F.B., Johnson, G.L., 2004. Dual-gauge system for measuring precipitation: Historical development and use. Journal of Hydrologic Engineering, 9(5): 350-359, doi: 10.1061/(ASCE)1084-0699(2004)9:5(350).

Harmel, R., Cooper, R., Slade, R., Haney, R., Arnold, J., 2006. Cumulative uncertainty in measured streamflow and water quality data for small watersheds. Transactions-American Society of Agricultural Engineers, 49(3): 689, doi: 10.13031/2013.20488.

Hevesi, J.A., Flint, A.L., Flint, L.E., 2003. Simulation of net infiltration and potential recharge using a distributed-parameter watershed model of the Death Valley region, Nevada and California. US Department of the Interior, US Geological Survey, Stable URL: http://pubs.usgs.gov/wri/wri034090/.

Hillel, D.,1998. Redistribution of water in soil. In *Environmental Soil Physics* (pp. 449-470). San Diego, California, Academic Press.

Hogan, J.F., Phillips, F.M., Scanlon, B.R., 2004. Groundwater recharge in a desert environment: the southwestern United States, 9. American Geophysical Union, doi: 10.1029/WS009.

Ivans, S., Hipps, L., Leffler, A.J., Ivans, C.Y., 2006. Response of water vapor and CO2 fluxes in semiarid lands to seasonal and intermittent precipitation pulses. Journal of Hydrometeorology, 7(5): 995-1010, doi: 10.1175/JHM545.1.

Jackson, R. et al., 1996. A global analysis of root distributions for terrestrial biomes. Oecologia, 108(3): 389-411, doi: 10.1007/BF00333714.

Jensen, M.E., Burman, R.D., Allen, R.G. eds., 1990. Evapotranspiration and irrigation water requirements, Manual of Practice No. 70, ASCE, New York. 360 pp.

Jie, Z., van Heyden, J., Bendel, D., Barthel, R., 2011. Combination of soil-water balance models and water-table fluctuation methods for evaluation and improvement of groundwater recharge calculations. Hydrogeology Journal, 19(8): 1487-1502, doi: 10.1007/s10040-011-0772-8.

Katsuyama, M., Tani, M., Nishimoto, S., 2010. Connection between streamwater mean residence time and bedrock groundwater recharge/discharge dynamics in weathered granite catchments. Hydrological processes, 24(16): 2287-2299, doi: 10.1002/hyp.7741.

Kelleners, T.J., Chandler, D.G., McNamara, J.P., Gribb, M.M., Seyfried, M.S., 2009. Modeling the Water and Energy Balance of Vegetated Areas with Snow Accumulation. Vadose Zone Journal, 8(4): 1013-1030, doi: 10.2136/vzj2008.0183.

Kelleners, T.J., Chandler, D.G., McNamara, J.P., Gribb, M.M., Seyfried, M.S., 2010. Modeling Runoff Generation on in a Small Snow-Dominated Mountainous Catchment. Vadose Zone Journal, 9(3): 517-527, doi: 10.2136/vzj2009.0033.

Kirchner, J.W., 2009. Catchments as simple dynamical systems: Catchment characterization, rainfall-runoff modeling, and doing hydrology backward. Water Resources Research, 45(2), doi: 10.1029/2008WR006912.

Knowles, N., Cayan, D.R., 2004. Elevational dependence of projected hydrologic changes in the San Francisco estuary and watershed. Climatic Change, 62(1-3): 319-336, doi: 10.1023/B:CLIM.0000013696.14308.b9.

Kormos, P. et al., 2014a. Soil, snow, weather, and sub-surface storage data from a mountain catchment in the rain–snow transition zone. Earth System Science Data, 6(1): 165-173, doi: 10.5194/essdd-6-811-2013.

Kormos, P.R. et al., 2014b. Snow distribution, melt and surface water inputs to the soil in the mountain rain-snow transition zone. Journal of Hydrology, 519(A): 190-204, doi: 10.1016/j.jhydrol.2014.06.051.

Krestovskiy, O., Postnikov, A., Sergeyeva, A., 1979. Estimation of evaporation from forest in early spring. Sov. Hdrol, 18: 181-186.

Kumar, M., Marks, D., Dozier, J., Reba, M., Winstral, A., 2013. Evaluation of distributed hydrologic impacts of temperature-index and energy-based snow models. Advances in Water Resources, 56: 77-89, doi: 10.1016/j.advwatres.2013.03.006.

Kunkel, M.L., Flores, A.N., Smith, T.J., McNamara, J.P., Benner, S.G., 2011. A simplified approach for estimating soil carbon and nitrogen stocks in semi-arid complex terrain. Geoderma, 165(1): 1-11, doi: 10.1016/j.geoderma.2011.06.011.

Kutilek, M., Nielsen, D.R., Soil Hydrology: texbook for students of soil science, agriculture, forestry, geoecology, hydrology, geomorphology and other related disciplines. Catena Verlag, Cremlingen, Germany. 370 pp.

Ladson, A.R., Lander, J.R., Western, A.W., Grayson, R.B., Zhang, L., 2006. Estimating extractable soil moisture content for Australian soils from field measurements. Australian Journal of Soil Research 44(5): 531-541, doi: 10.1071/SR04180.

Lettenmaier, D.P., Gan, T.Y., 1990. Hydrologic sensitivities of the Sacramento River basin, California, to global warming. Water Resources Research, 26(1): 69-86, doi: 10.1029/WR026i001p00069.

Lutz, J.A., Martin, K.A., Lundquist, J.D., 2012. Using fiber-optic distributed temperature sensing to measure ground surface temperature in thinned and unthinned forests. Northwest Science, 86(2): 108-121, doi: 10.3955/046.086.0203.

Marks, D., Winstral, A., 2001. Comparison of snow deposition, the snow cover energy balance, and snowmelt at two sites in a semiarid mountain basin. Journal of Hydrometeorology, 2(3): 213-227, doi:10.1175/1525-7541(2001)002<0213:COSDTS>2.0.CO;2.

Marks, D., Winstral, A.H., Reba, M.L., Pomeroy, J., Kumar, M., 2013. An evaluation of methods for determining during-storm precipitation phase and the rain/snow transition elevation at the surface in a mountain basin. Advances in Water Resources(55): 98-110, doi: 10.1016/j.advwatres.2012.11.012.

McCabe, G.J., Hay, L.E., Clark, M.P., 2007. Rain-on-snow events in the western United States. Bulletin of the American Meteorological Society, 88(3): 319-328, doi: 10.1175/BAMS-88-3-319.

McNamara, J., Chandler, D., Seyfried, M., Achet, S., 2005. Soil moisture states, lateral flow, and streamflow generation in a semi-arid, snowmelt-driven catchment. Hydrological Processes, 19(20): 4023-4038, doi: 10.1002/hyp.5869.

McNamara, J.P. et al., 2011. Storage as a Metric of Catchment Comparison. Hydrological Processes, 25(21): 3364-3371, doi: 10.1002/hyp.8113.

Miller, C.R., Routh, P.S., Brosten, T.R., McNamara, J.P., 2008. Application of time-lapse ERT imaging to watershed characterization. Geophysics, 73(3): G7-G17, doi: 10.1190/1.2907156.

Mote, P.W., Hamlet, A.F., Clark, M.P., Lettenmaier, D.P., 2005. Declining mountain snowpack in western North America, URI: http://hdl.handle.net/1957/28018.

Murray, C., Buttle, J., 2005. Infiltration and soil water mixing on forested and harvested slopes during spring snowmelt, Turkey Lakes Watershed, central Ontario. Journal of Hydrology, 306(1): 1-20, doi: 10.1016/j.jhydrol.2004.08.032.

Nayak, A., Marks, D., Chandler, D.G., Seyfried, M., 2010. Long-term snow, climate, and streamflow trends at the Reynolds Creek Experimental Watershed, Owyhee Mountains, Idaho, United States. Water Resources Research, 46: 15, doi: 10.1029/2008WR007525.

Nolan, B.T. et al., 2007. Factors influencing ground-water recharge in the eastern United States. Journal of Hydrology, 332(1): 187-205, doi: 10.1016/j.jhydrol.2006.06.029.

Nolin, A.W., Daly, C., 2006. Mapping “at risk” snow in the Pacific Northwest. Journal of Hydrometeorology, 7(5): 1164-1171, doi: 10.1175/JHM543.1.

Papalexiou, S.-M., Koutsoyiannis, D., Montanari, A., 2011. Can a simple stochastic model generate rich patterns of rainfall events? Journal of Hydrology, 411(3): 279-289, doi: 10.1016/j.jhydrol.2011.10.008.

Priestley, C.H.B., Taylor, R.J., 1972. On the Assessment of Surface Heat Flux and Evaporation Using Large-Scale Parameters. Monthly Weather Review, 100(2): 81-92, doi: 10.1175/1520-0493(1972)100<0081:OTAOSH>2.3.CO;2.

Ragab, R., Finch, J., Harding, R., 1997. Estimation of groundwater recharge to chalk and sandstone aquifers using simple soil models. Journal of Hydrology, 190(1): 19-41, doi: 10.1016/S0022-1694(96)03067-3.

Reba, M. L., Marks, D., Winstral, A., Link, T. E., Kumar, M., 2011. Sensitivity of the snowcover energetics in a mountain basin to variations in climate. Hydrological Processes, 25(21): 3312-3321, doi: 10.1002/hyp.8155.

Ritchie, J.T., 1972. Model for predicting evaporation in from a row crop with incomplete cover. Water Resources Research, 8(5): 1204-1213, doi: 10.1029/WR008i005p01204.

Ritchie, J.T. 1981. Soil water availability. Plant and Soil 58(1): 327-338, doi: 10.1007/BF02180061.

Ritchie, J.T., 1985. A user-oriented model of the soil water balance in wheat. In *Wheat Growth and Modelling*. Day, W., Atkin, R.K. eds., NATO-ASI Series-Series A Life Sciences, 86: 293-305: doi: 10.1007/978-1-4899-3665-3_27.

Rose, C.W., 1984. Modelling evapotranspiration: An approach to heterogeneous communities. Agricultural Water Management, 8(1–3): 203-221, doi: 10.1016/0378-3774(84)90054-4.

Sammis, T.W., Evans, D.D., Warrick, A., 1982. Comparison of methods to estimate deep percolation rates. Journal of the American Water Resources Association, 18: 465–470, doi: 10.1111/j.1752-1688.1982.tb00013.x.

Saxton, K., Rawls, W.J., 2006. Soil water characteristic estimates by texture and organic matter for hydrologic solutions. Soil Science Society of America Journal. 70(5): 1569-1578, doi: 10.2136/sssaj2005.0117.

Saxton, K., Rawls, W.J., Romberger, J., Papendick, R., 1986. Soil Science Society of America Journal, 50(4): 1031-1036, doi:10.2136/sssaj1986.03615995005000040039x.

Scanlon, B.R., Healy, R.W., Cook, P.G., 2002. Choosing appropriate techniques for quantifying groundwater recharge. Hydrogeology Journal, 10(1): 18-39, doi: 10.1007/s10040-001-0176-2.

Scanlon, B.R. et al., 2006. Global synthesis of groundwater recharge in semiarid and arid regions. Hydrological Processes, 20(15): 3335-3370, doi: 10.1002/hyp.6335.

Selle, B., Minasny, B., Bethune, M., Thayalakumaran, T., Chandra, S., 2011. Applicability of Richards' equation models to predict deep percolation under surface irrigation. Geoderma, 160(3): 569-578, doi: 10.1016/j.geoderma.2010.11.005.

Seyfried, M., 2003. Incorporation of remote sensing data in an upscaled soil water model. CRC Press: New York.

Seyfried, M.S., Marks, D.G., Chandler, D.G., 2011. Long-term soil water trends across a 1000 m elevation gradient. Vadose Zone Journal, 10(4): 1275-1285 doi:10.2136/vzj2011.0014.

Seyfried, M., Murdock, M., 2001. Response of a new soil water sensor to variable soil, water content, and temperature. Soil Science Society of America Journal, 65(1): 28-34, doi: 10.2136/sssaj2001.65128x.

Seyfried, M.S., Grant, L.E., Marks, D., Winstral, A., McNamara, J., 2009. Simulated soil water storage effects on streamflow generation in a mountainous snowmelt environment, Idaho, USA. Hydrological Processes, 23(6): 858-873, doi: 10.1002/hyp.7211.

Sheffer, N.A. et al., 2011. Integrated cave drip monitoring for epikarst recharge estimation in a dry Mediterranean area, Sif Cave, Israel. Hydrological Processes, 25(18): 2837-2845, doi: 10.1002/hyp.8046.

Shuttleworth, W.J., Maidment, D., 1992. Evaporation. McGraw-Hill Inc, ISBN0-07-039732-5.

Simmers, I., 1998. Groundwater recharge: an overview of estimation ‘problems’ and recent developments. Geological Society, London, Special Publications, 130(1): 107-115, doi: 10.1144/GSL.SP.1998.130.01.10.

Smith, T.J. et al., 2011. Small soil storage capacity limits benefit of winter snowpack to upland vegetation. Hydrological Processes, 25(25): 3858-3865, doi: 10.1002/hyp.8340.

Sorensen, J., Finch, J., Ireson, A., Jackson, C., 2014. Comparison of varied complexity models simulating recharge at the field scale. Hydrological Processes, 28(4): 2091-2102, doi: 10.1002/hyp.9752.

Spence, C., 2007. On the relation between dynamic storage and runoff: A discussion on thresholds, efficiency, and function. Water Resources Research, 43(12), doi: 10.1029/2006WR005645.

Spence, C. et al., 2010. Storage dynamics and streamflow in a catchment with a variable contributing area. Hydrological Processes, 24(16): 2209-2221, doi: 10.1002/hyp.7492.

Spence, L.E., 1937. Root Studies of Important Range Plants of the Boise River Watershed. Journal of Forestry, 35(8): 747-754, URL: http://www.ingentaconnect.com/content/saf/jof/1937/00000035/00000008/art00012.

Steinwand, A., Harrington, R., Or, D., 2006. Water balance for Great Basin phreatophytes derived from eddy covariance, soil water, and water table measurements. Journal of Hydrology, 329(3): 595-605, doi: 10.1016/j.jhydrol.2006.03.013.

Sutanudjaja, E., Van Beek, L., De Jong, S., Van Geer, F., Bierkens, M., 2011. Large-scale groundwater modeling using global datasets: a test case for the Rhine-Meuse basin. Hydrology and Earth System Sciences, 15(9): 2913-2935, doi: 10.5194/hess-15-2913-2011.

Taucer, P., Munster, C., Wilcox, B., Owens, M., Mohanty, B., 2008. Large-scale rainfall simulation experiments on juniper rangelands. Transactions of the ASABE, 51: 1951-1961, doi: 10.13031/2013.25400.

Tesfa, T.K., Tarboton, D.G., Chandler, D.G., McNamara, J.P., 2009. Modeling soil depth from topographic and land cover attributes. Water Resources Research, 45, doi: 10.1029/2008WR007474.

Thoma, M.J., McNamara, J.P., Gribb, M.M., Benner, S.G., 2011. Seasonal recharge components in an urban/agricultural mountain front aquifer system using noble gas thermometry. Journal of Hydrology, 409(1-2): 118-127, doi: 10.1016/j.jhydrol.2011.08.003.

Topp, G., Davis, J., Annan, A.P., 1980. Electromagnetic determination of soil water content: Measurements in coaxial transmission lines. Water resources research, 16(3): 574-582, doi: 10.1029/WR016i003p00574.

Tromp-van Meerveld, H., Peters, N., McDonnell, J., 2007. Effect of bedrock permeability on subsurface stormflow and the water balance of a trenched hillslope at the Panola Mountain Research Watershed, Georgia, USA. Hydrological Processes, 21(6): 750-769, doi: 10.1002/hyp.6265.

Van der Lee, J., Gehrels, J., 1997. Modelling of groundwater recharge for a fractured dolomite aquifer under semi-arid conditions. Recharge of phreatic aquifers in (semi-) arid areas. IAH Int Contrib Hydrogeol, 19: 129-144.

Veihmeyer, F., Hendrickson, A., 1931. The moisture equivalent as a measure of the field capacity of soils. Soil Science, 32(3): 181-194.

Wang, L., Wei, S., Horton, R., Shao, M.a., 2011. Effects of vegetation and slope aspect on water budget in the hill and gully region of the Loess Plateau of China. Catena, 87(1): 90-100, doi: 10.1016/j.catena.2011.05.010.

Warrick, A.W., Nielsen, D.R., 1980. Spatial variability of soil physical properties in the field. In *Applications of Soil Physics*, Hillel, D. Ed. Academic Press, New York, pp. 319-344.

Williams, C.J., McNamara, J.P., Chandler, D.G., 2009. Controls on the temporal and spatial variability of soil moisture in a mountainous landscape: the signature of snow and complex terrain. Hydrology and Earth System Sciences, 13(7): 1325-1336, doi: 10.5194/hess-13-1325-2009.

Willmott, C.J., Rowe, C.M., Mintz, Y., 1985. Climatology of the terrestrial seasonal water cycle. Journal of Climatology, 5(6): 589-606, doi: 10.1002/joc.3370050602.

Wilson, J.L., Guan, H., 2004. Mountain-Block Hydrology and Mountain-Front Recharge. Groundwater recharge in a desert environment: the southwestern United States: 113-137.

Winstral, A., Marks, D., 2002. Simulating wind fields and snow redistribution using terrain-based parameters to model snow accumulation and melt over a semi-arid mountain catchment, Hydrological Processes, 16(18): 3585–3603. doi: 10.1002/hyp.1238.

Winstral, A., Marks, D., Gurney, R., 2013. Simulating wind-affected snow accumulations at catchment to basin scales. Advances in Water Resources, 55: 64-79, doi: 10.1016/j.advwatres.2012.08.011.

Wood, W.W., 1999. Use and Misuse of the Chloride-Mass Balance Method in Estimating Ground Water Recharge. Groundwater, 37(1): 2-3, doi: 10.1111/j.1745-6584.1999.tb00949.x.

Wight, J.R., Hanks, R.J., 1981. A water-balance, climate model for range herbage production. Journal of Range Management, 34(4): 307-311, Article Stable URL: http://www.jstor.org/stable/3897857.

Yenko, M.K., 2003. Hydrometric and geochemical evidence of streamflow sources in the Upper Dry Creek Experimental Watershed, southwestern Idaho, Boise State University.

Zhang, L., Potter, N., Hickel, K., Zhang, Y., Shao, Q., 2008. Water balance modeling over variable time scales based on the Budyko framework–Model development and testing. Journal of Hydrology, 360(1): 117-131, doi: 10.1016/j.jhydrol.2008.07.021.

Tables

Table 1. List of model parameters with a brief description of the methods used to obtain parameter values.

Parameter	Method
Field Capacity (FC)	Empirical from measured annual soil moisture data (Figure 3)
Plant Extraction Limit (PEL)	Empirical from measured annual soil moisture data (Figure 3)
Soil Saturation (SAT)	Empirical from measured texture data (Saxton, 1986)
Redistribution Time (RDT)	Literature (Seyfried et al. 2009) and Data observation
LAI Shape Factors (C & D)	Held constant to ensure quick green up and dry down by August.
LAI Start Day of Year (GS_{st})	Slope-averaged snow meltout date from *Isnobal*
LAI Maximum Value (LAI_{max})	Optimized *see* Parameterizing the Soil Ecohydraulic Model
LAI Minimum Value (LAI_{min})	Optimized *see* Parameterizing the Soil Ecohydraulic Model
LAI Peak Day of Year (GS_{pk})	Optimized *see* Parameterizing the Soil Ecohydraulic Model

Table 2. List of LAI time series parameters and values used on the two dominant slopes in Treeline.

Parameter	Northeast Facing Slope (NE)	Southwest Facing Slope (SW)
growing season start (GS_{st})	111	97
growing season peak (GS_{pk})	185	198
C	0.3	0.3
D	5	7
leaf area index maximum (LAI_{max})	1.0782	0.9125
leaf area index minimum (LAI_{min})	0.2741	0.1436

Table 3. Annual water balance terms and uncertainties from WY2011 at TREELINE.

	Estimate (mm)	Uncertainty (mm)
Precipitation (distributed)	859	-
SWI	810	32
Soil Water Storage	-	19
Q	-325	33
ET	-196	6
BI	-289	50
DR	-614	38

Figures

Figure 1. Location map of Treeline catchment showing location of weather station, flume, soil moisture profiles, and *SEM* model points.

Figure 2. Schematic of the spatial distribution of *Isnobal* model pixels versus the Theissen polygons representing points where *SEM* model runs. SWI from *Isnobal* pixels are averaged over the 57 Theissen polygons then summed over the daily time step to get a daily snow water input. Theissen polygons are color coded by soil depth measured at the model point.

Figure 3. a) Modeled snow water equivalent at the weather station with ROS events highlighted. b) Daily minimum and maximum air temperature and c) daily incoming shortwave radiation as input to *SEM*.

Figure 4. Measured soil moisture from the northeast facing slope including modeled results SEM8. Horizontal lines show the empirical values of field capacity (FC) and plant extraction limit (PEL) parameters.

Figure 5. Field capacity (FC) vs. soil depth relationship for the northeast facing and southwest facing slopes.

Figure 6. a) Modeled cumulative SWI from NE and SW slopes showing the timing of ROS events. b) Cumulative modeled soil drainage to the soil bedrock interface (Dr_t) on NE and SW slopes. Cumulative streamflow (Q_t) is also depicted. c) Incremental modeled daily Dr_t on NE and SW slopes.

Figure 7. Time series of a) catchment soil storage, b) measured discharge and modeled soil drainage to the soil bedrock interface (Dr_t), and c) calculated bedrock infiltration (BI_t) compared to modeled evapotranspiration (ET_t).

Figure 8. Lateral fluxes on the NE slope measured below the soil surface at 4 cm and 125 cm depths and at the soil bedrock interface. Soil moisture at several depths is also included from a nearby soil profile N3.

Figure 9. Measured and modeled soil water storage for each of the soil profiles at the Treeline catchment. Modeled results are from the closest modeled point and modeled depths are modified to match the measured soil depth at the soil pits for comparison.

Figure 10. Distributed two week summed soil drainage to the soil bedrock interface (Dr_t) at the Treeline catchment for WY2011.

Figure 11. Distributed cumulative drainage to the soil bedrock interface (Dr_t) every two weeks at Treeline during WY2011.

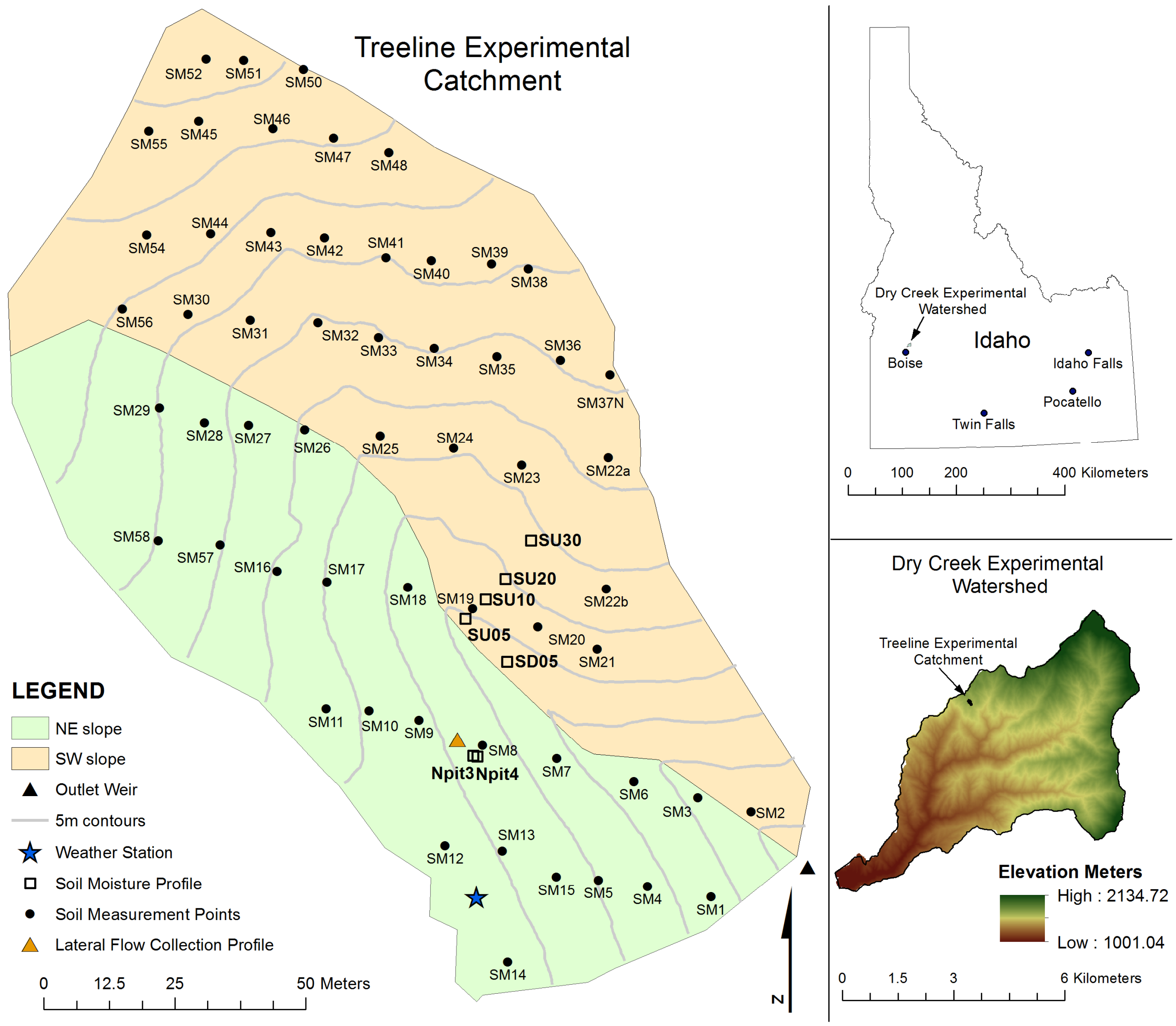

Treeline Experimental Catchment
SM52
SM51
SM50
SM46
SM55
SM45
SM47
SM48
SM44
SM54
SM43
SM42
SM41
SM40
SM39
SM38
SM30
SM56
SM31
SM32
SM33
SM34
SM35
SM36
SM37N
SM29
SM28
SM27
SM26
SM25
SM24
SM23
SM22a
SM58
SM57
SM16
SM17
SU30
SU20
SM18
SM19
SU10
SM22b
SU05
SM20
SD05
SM21
SM11
SM10
SM9
SM8
Npit3
Npit4
SM7
SM6
SM3
SM2
SM13
SM12
SM15
SM5
SM4
SM1
SM14
LEGEND
NE slope
SW slope
Outlet Weir
5m contours
Weather Station
Soil Moisture Profile
Soil Measurement Points
Lateral Flow Collection Profile
0 12.5 25 50 Meters
N
Dry Creek Experimental Watershed
Idaho
Boise
Idaho Falls
Pocatello
Twin Falls
0 100 200 400 Kilometers
Dry Creek Experimental Watershed
Treeline Experimental Catchment
Elevation Meters
High : 2134.72
Low : 1001.04
0 1.5 3 6 Kilometers

1296 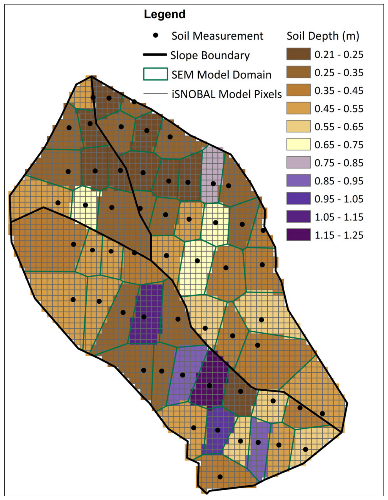
Legend
Soil Measurement
Slope Boundary
SEM Model Domain
iSNOBAL Model Pixels
Soil Depth (m)
0.21 - 0.25
0.25 - 0.35
0.35 - 0.45
0.45 - 0.55
0.55 - 0.65
0.65 - 0.75
0.75 - 0.85
0.85 - 0.95
0.95 - 1.05
1.05 - 1.15
1.15 - 1.25

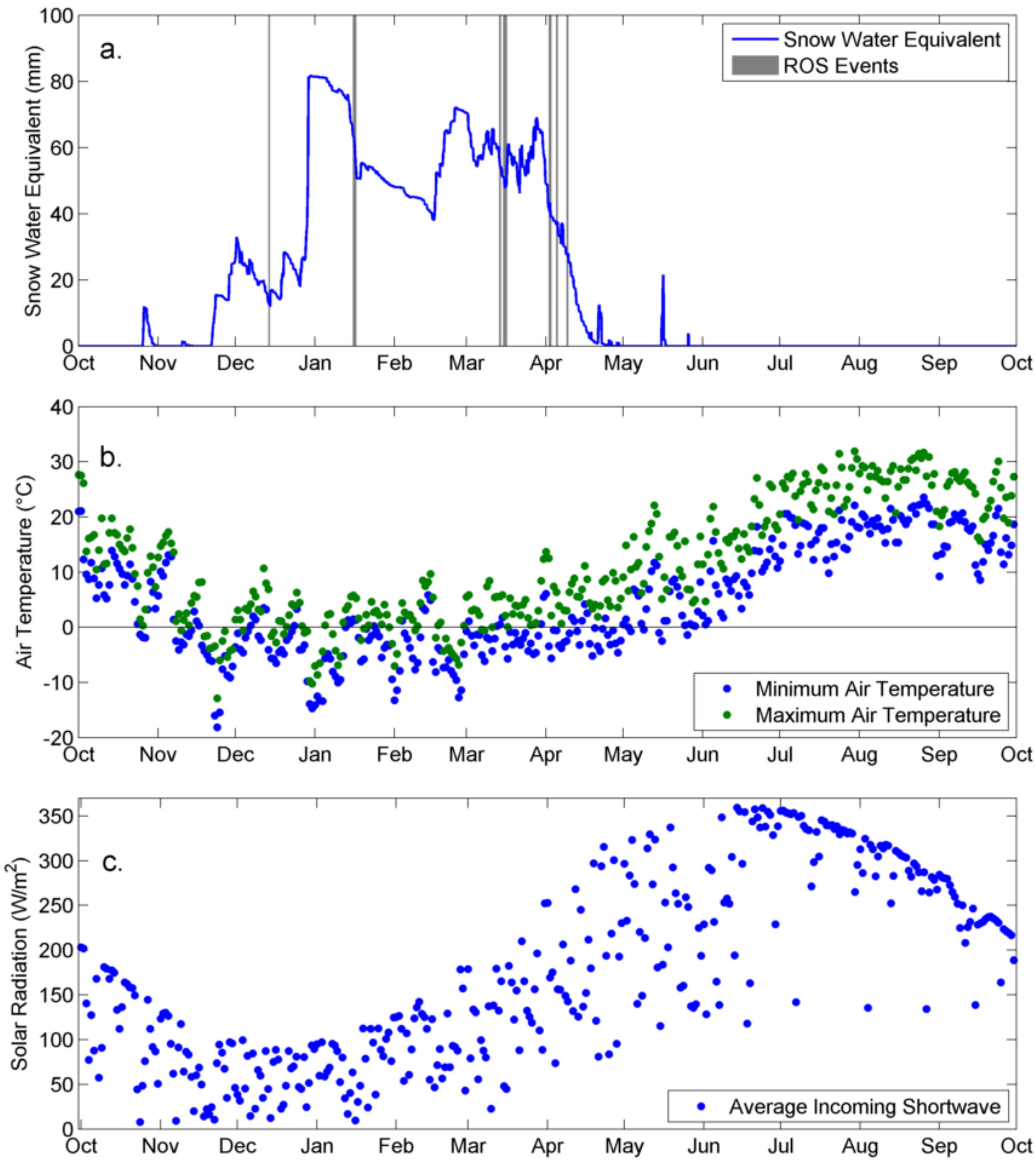
a.
Snow Water Equivalent
ROS Events
Snow Water Equivalent (mm)
b.
Air Temperature (°C)
Minimum Air Temperature
Maximum Air Temperature
c.
Solar Radiation (W/m2)
Average Incoming Shortwave
Oct
Nov
Dec
Jan
Feb
Mar
Apr
May
Jun
Jul
Aug
Sep
Oct

1297

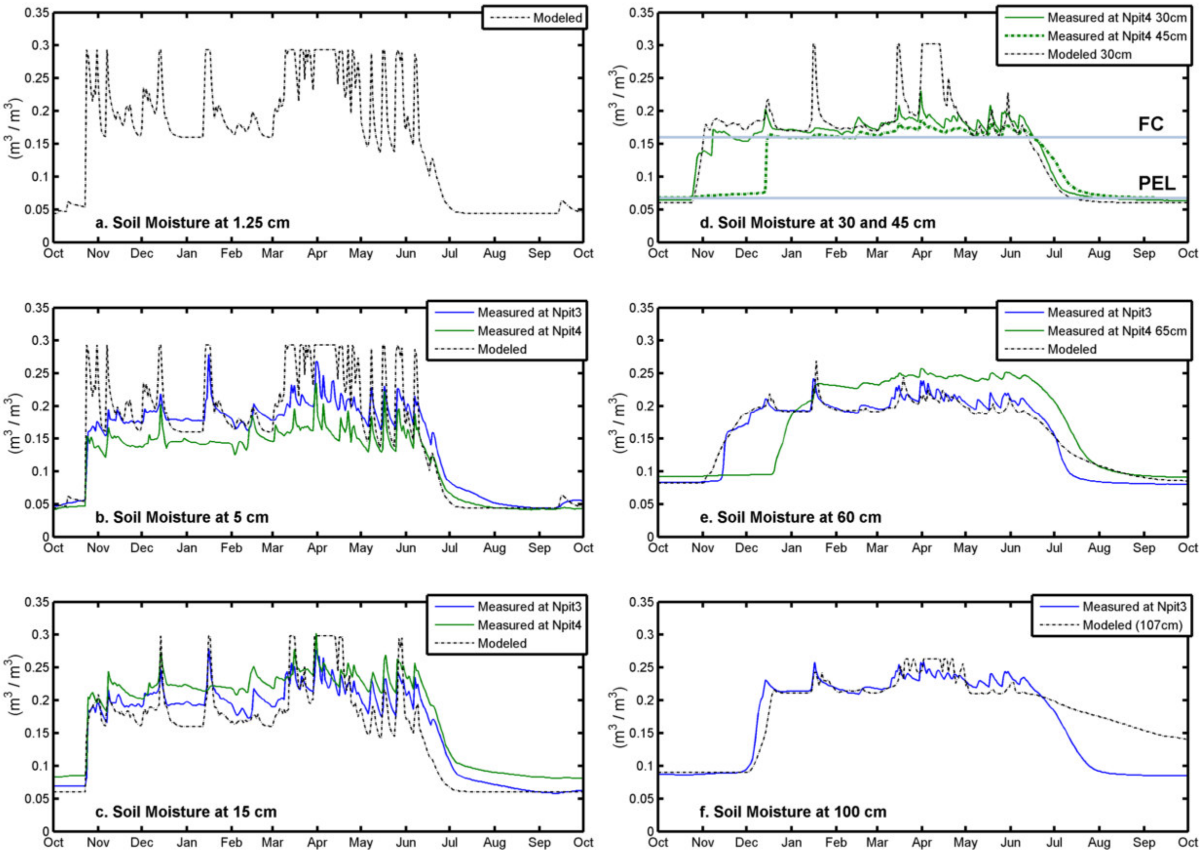
Modeled
a. Soil Moisture at 1.25 cm
Measured at Npit4 30cm
Measured at Npit4 45cm
Modeled 30cm
FC
PEL
d. Soil Moisture at 30 and 45 cm
Measured at Npit3
Measured at Npit4
Modeled
b. Soil Moisture at 5 cm
Measured at Npit3
Measured at Npit4 65cm
Modeled
e. Soil Moisture at 60 cm
Measured at Npit3
Measured at Npit4
Modeled
c. Soil Moisture at 15 cm
Measured at Npit3
Modeled (107cm)
f. Soil Moisture at 100 cm
(m3 / m3)
Oct
Nov
Dec
Jan
Feb
Mar
Apr
May
Jun
Jul
Aug
Sep
Oct

1298
1299

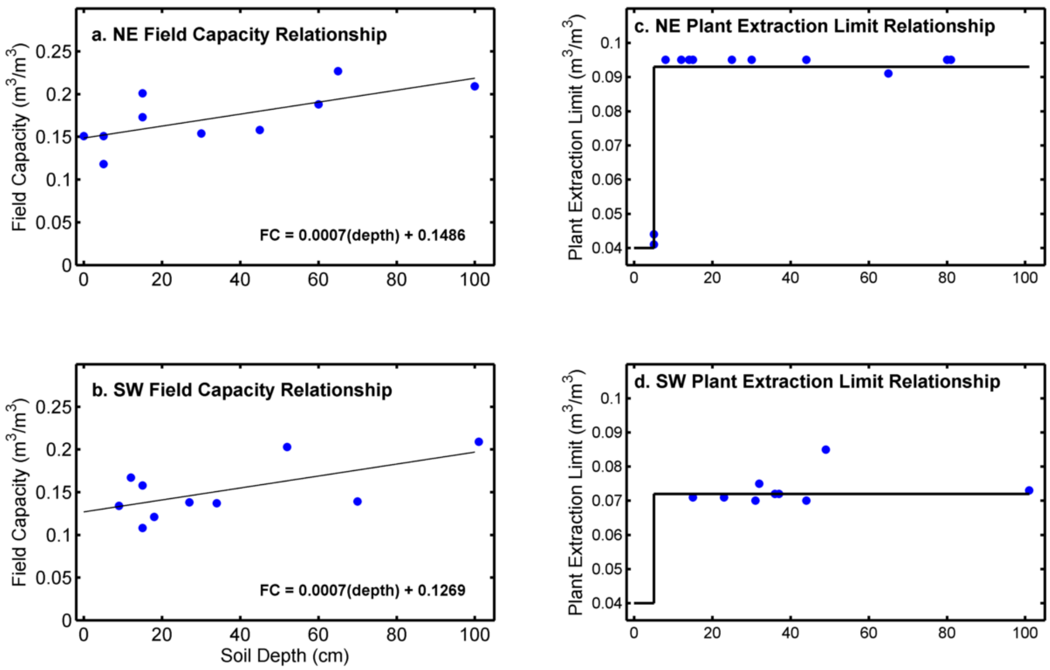
a. NE Field Capacity Relationship
Field Capacity (m^3/m^3)
FC = 0.0007(depth) + 0.1486
b. SW Field Capacity Relationship
FC = 0.0007(depth) + 0.1269
Soil Depth (cm)
c. NE Plant Extraction Limit Relationship
Plant Extraction Limit (m^3/m^3)
d. SW Plant Extraction Limit Relationship

1300
1301

1302

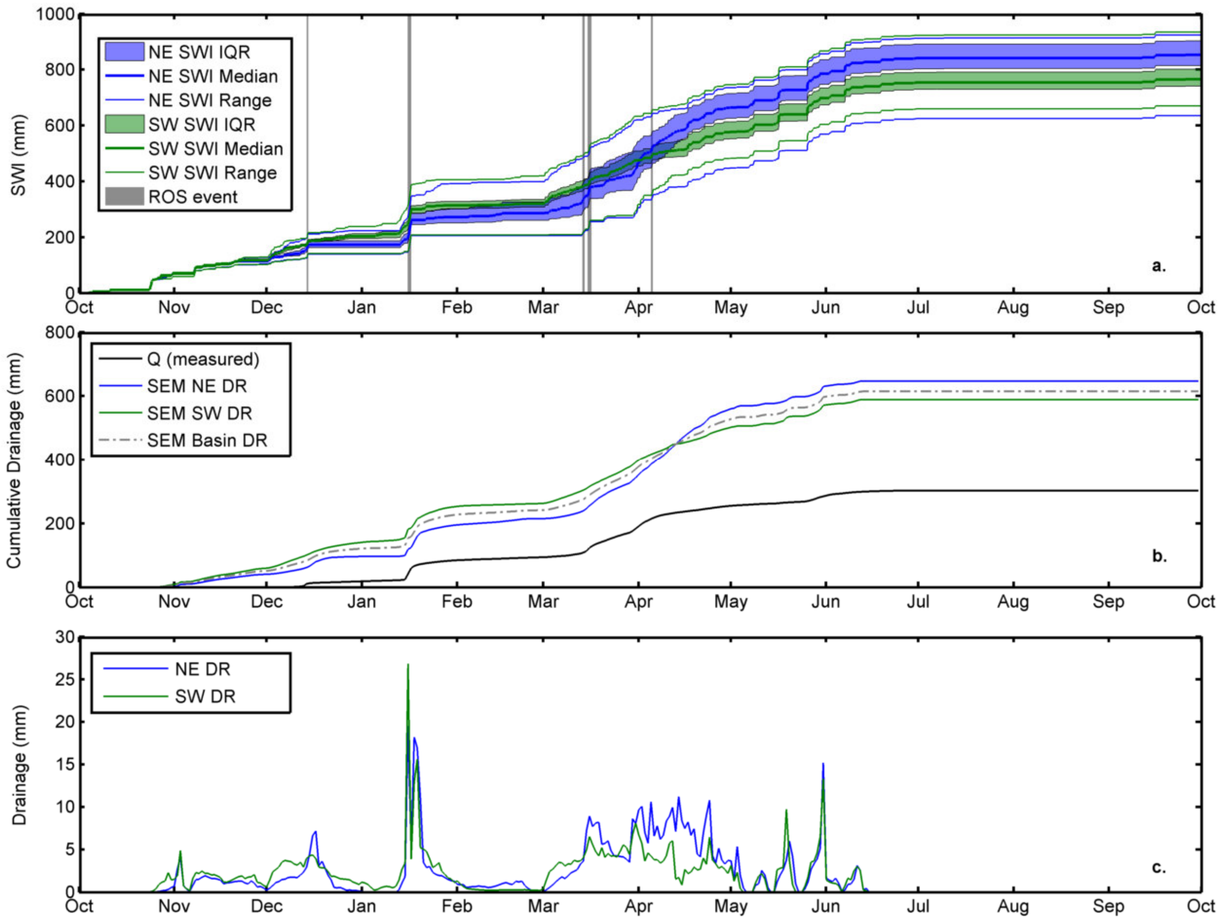
NE SWI IQR
NE SWI Median
NE SWI Range
SW SWI IQR
SW SWI Median
SW SWI Range
ROS event
SWI (mm)
a.
Q (measured)
SEM NE DR
SEM SW DR
SEM Basin DR
Cumulative Drainage (mm)
b.
NE DR
SW DR
Drainage (mm)
c.
Oct Nov Dec Jan Feb Mar Apr May Jun Jul Aug Sep Oct

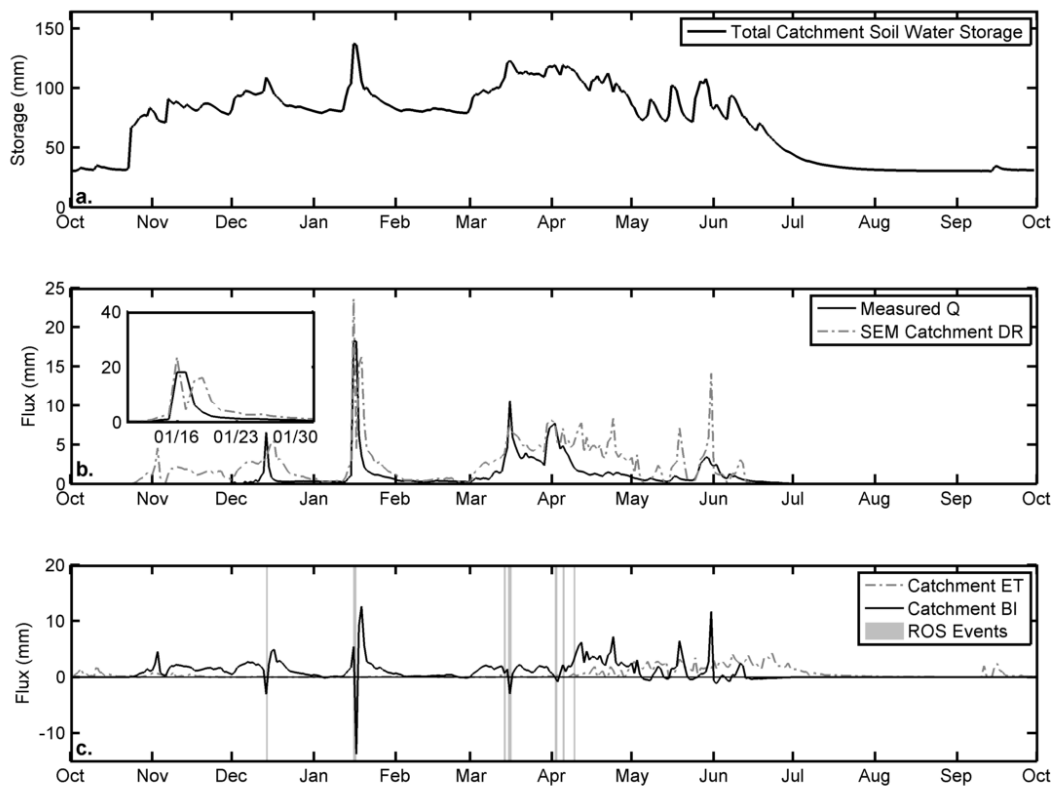

Total Catchment Soil Water Storage
Storage (mm)
150
100
50
0
a.
Oct
Nov
Dec
Jan
Feb
Mar
Apr
May
Jun
Jul
Aug
Sep
Oct
Measured Q
SEM Catchment DR
Flux (mm)
25
20
15
10
5
0
40
20
0
01/16
01/23
01/30
b.
Catchment ET
Catchment BI
ROS Events
20
10
0
-10
c.

1303
1304

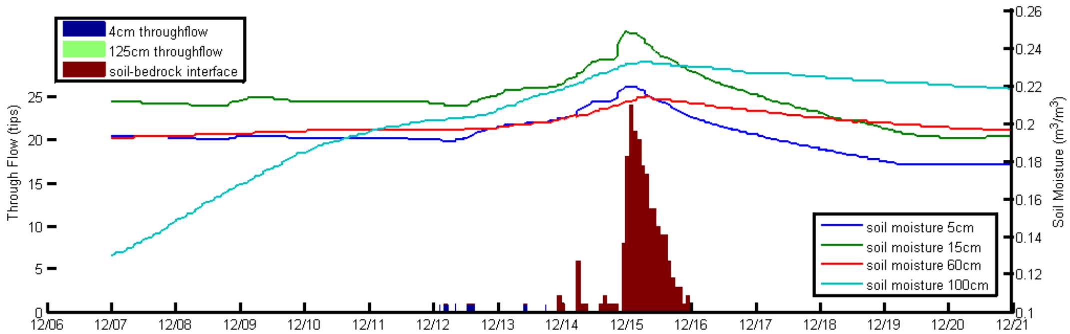
4cm throughflow
125cm throughflow
soil-bedrock interface
soil moisture 5cm
soil moisture 15cm
soil moisture 60cm
soil moisture 100cm
Through Flow (tips)
Soil Moisture (m3/m3)
0
5
10
15
20
25
0.1
0.12
0.14
0.16
0.18
0.2
0.22
0.24
0.26
12/06
12/07
12/08
12/09
12/10
12/11
12/12
12/13
12/14
12/15
12/16
12/17
12/18
12/19
12/20
12/21

1305
1306

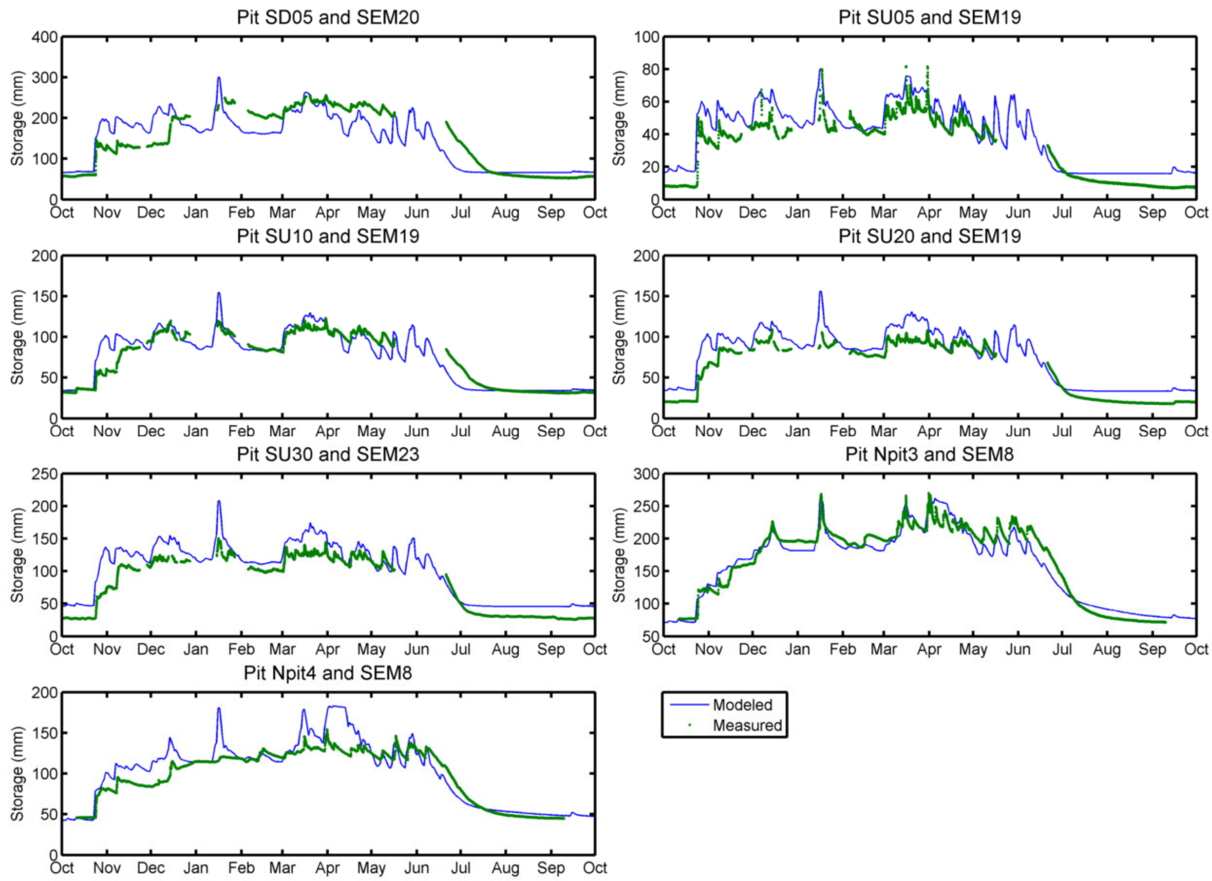
Pit SD05 and SEM20
Pit SU05 and SEM19
Pit SU10 and SEM19
Pit SU20 and SEM19
Pit SU30 and SEM23
Pit Npit3 and SEM8
Pit Npit4 and SEM8
Storage (mm)
Oct
Nov
Dec
Jan
Feb
Mar
Apr
May
Jun
Jul
Aug
Sep
Oct
Modeled
Measured

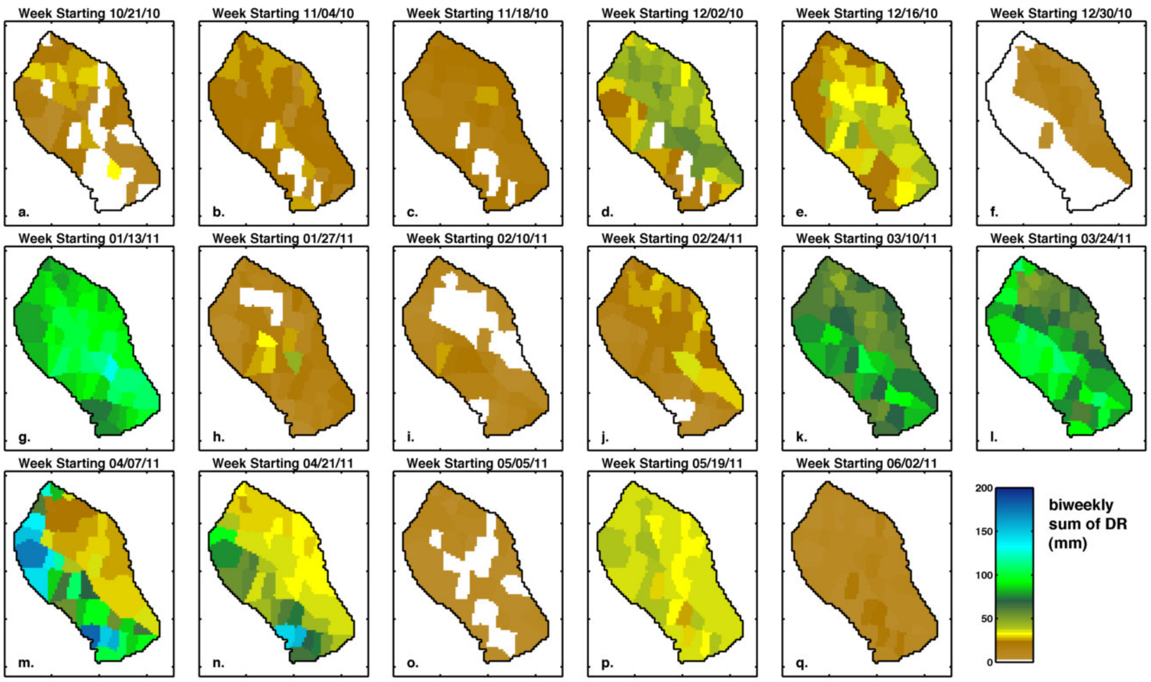
Week Starting 10/21/10
Week Starting 11/04/10
Week Starting 11/18/10
Week Starting 12/02/10
Week Starting 12/16/10
Week Starting 12/30/10
a.
b.
c.
d.
e.
f.
Week Starting 01/13/11
Week Starting 01/27/11
Week Starting 02/10/11
Week Starting 02/24/11
Week Starting 03/10/11
Week Starting 03/24/11
g.
h.
i.
j.
k.
l.
Week Starting 04/07/11
Week Starting 04/21/11
Week Starting 05/05/11
Week Starting 05/19/11
Week Starting 06/02/11
m.
n.
o.
p.
q.
200
150
100
50
0
biweekly
sum of DR
(mm)

1309
1310

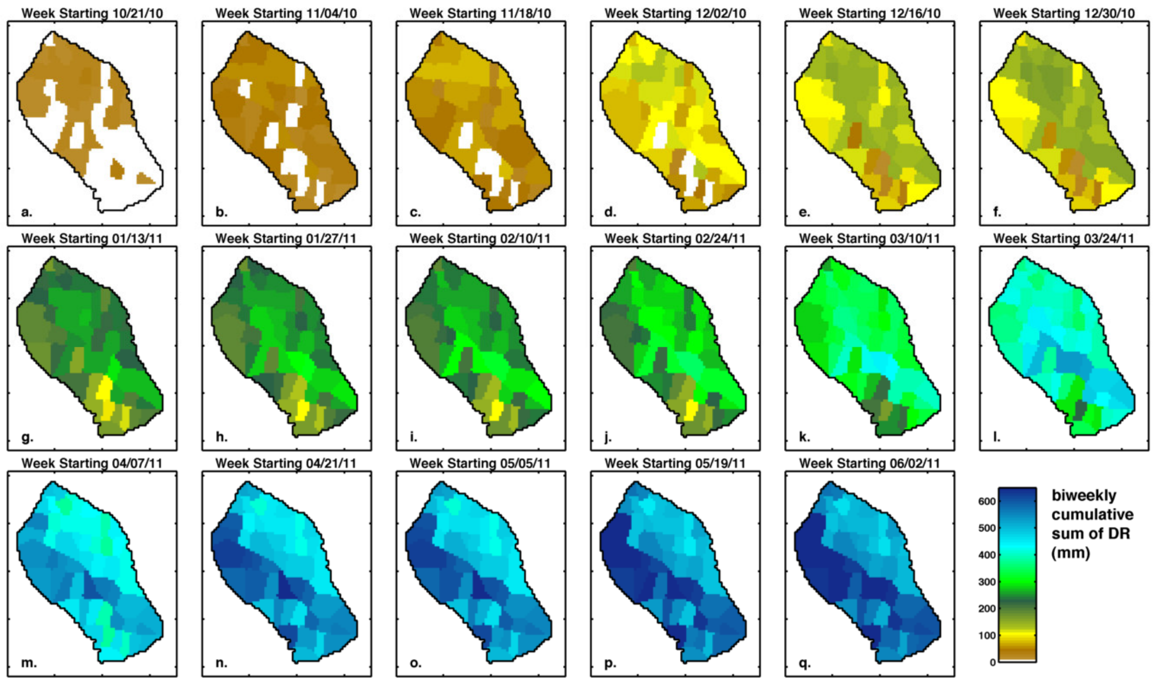
Week Starting 10/21/10
a.
Week Starting 11/04/10
b.
Week Starting 11/18/10
c.
Week Starting 12/02/10
d.
Week Starting 12/16/10
e.
Week Starting 12/30/10
f.
Week Starting 01/13/11
g.
Week Starting 01/27/11
h.
Week Starting 02/10/11
i.
Week Starting 02/24/11
j.
Week Starting 03/10/11
k.
Week Starting 03/24/11
l.
Week Starting 04/07/11
m.
Week Starting 04/21/11
n.
Week Starting 05/05/11
o.
Week Starting 05/19/11
p.
Week Starting 06/02/11
q.
600
500
400
300
200
100
0
biweekly
cumulative
sum of DR
(mm)

Parameter	Method
Field Capacity (FC)	Empirical from measured annual soil moisture data (Figure 3)
Plant Extraction Limit (PEL)	Empirical from measured annual soil moisture data (Figure 3)
Soil Saturation (SAT)	Empirical from measured texture data (Saxton, 1986)
Redistribution Time (RDT)	Literature (Seyfried et al. 2009) and Data observation
LAI Shape Factors (C & D)	Held constant to ensure quick green up and dry down by August.
LAI Start Day of Year (GS_{st})	Slope-averaged snow meltout date from *Isnobal*
LAI Maximum Value (LAI_{max})	Optimized *see* Parameterizing the Soil Ecohydraulic Model
LAI Minimum Value (LAI_{min})	Optimized *see* Parameterizing the Soil Ecohydraulic Model
LAI Peak Day of Year (GS_{pk})	Optimized *see* Parameterizing the Soil Ecohydraulic Model

ACCEPTED MANUSCRIPT

Table 2. Table 2. List of LAI time series parameters and values used on the two dominant slopes in Treeline.

Parameter	Northeast Facing Slope (NE)	Southwest Facing Slope (SW)
growing season start (GS_{st})	111	97
growing season peak (GS_{pk})	185	198
C	0.3	0.3
D	5	7
leaf area index maximum (LAI_{max})	1.0782	0.9125
leaf area index minimum (LAI_{min})	0.2741	0.1436

Table 3. Annual water balance terms and uncertainties from WY2011 at TL.

	Estimate (mm)	Uncertainty (mm)
Precipitation (distributed)	859	-
SWI	810	32
Soil Water Storage	-	19
Q	-325	33
ET	-196	6
BI	-289	50
DR	-614	38

Highlights for Kormos, et al.: Bedrock infiltration estimates from a catchment water storage-based modeling approach in the rain snow transition zone.

- We estimate bedrock infiltration from a catchment in the rain-snow transition zone.
- Our combined field and modeling approach focuses on catchment water storage.
- A physically based snow model is loosely coupled to a capacitance based soil model.
- Peaks in soil drainage and bedrock infiltration coincide with rain on snow events.
- Southwest soils drain more often. Northeast soils contribute more total drainage.

ACCEPTED MANUSCRIPT